Composites Part B 312 (2026) 113349

Contents lists available at ScienceDirect

Composites Part B

journal homepage: www.elsevier.com/locate/compositesb

# Moisture absorption behavior of sheet molding compound thermoplastic composites and its influence on the impact performance of a battery housing

Aikaterini Fragiadaki, Konstantinos Tserpes *

*Laboratory of Technology & Strength of Materials, Department of Mechanical Engineering & Aeronautics, University of Patras, Patras, 26500, Greece*

A R T I C L E I N F O

*Keywords:*
Moisture absorption
Desorption
Fick
SMC
Thermoplastic
Housing
Impact

A B S T R A C T

Nowadays, composite materials are increasingly used for electric vehicle (EV) battery housings due to their superior specific properties, improving the overall safety and performance of the vehicles. This study investigates the long-term moisture absorption behaviour of a flame-retardant thermoplastic sheet molding compound (SMC) composite and its implications regarding the crash performance of a battery housing. Specimens were subjected to immersion in deionized water at 25 °C for up to 3000 h, followed by desorption, revealing an initial Fickian diffusion stage, reaching an equilibrium moisture content of 0.75 wt %, followed by non-Fickian behaviour associated with matrix plasticization and interfacial damage. Mechanical testing confirmed substantial property degradation, with tensile and flexural strengths reduced by approximately 50 % at saturation, while desorption resulted in partial recovery indicating irreversible microstructural damage. Diffusion models based on Fick's law were developed to predict moisture absorption, while linear and exponential degradation laws were employed to describe property evolution as a function of moisture content. The experimentally calibrated degradation model was subsequently integrated into LS-DYNA simulations to assess the impact response of the battery housing structure. Numerical results demonstrate that moisture-induced degradation significantly reduces the energy absorption capability and increases deformation of the housing, particularly under higher impact velocities, leading to increased displacement of the internal cell pack. This proposed coupled experimental and numerical framework provides a practical methodology for incorporating environmental aging effects into the crashworthiness assessment and design of EV battery enclosures, with regards to a safety-oriented approach.

## 1. Introduction

The transition toward electric mobility has intensified the demand for lightweight and durable battery enclosures. Beyond structural protection, the battery housing must also ensure thermal stability, flame resistance, and long-term reliability under real-world service conditions. Composite materials are gaining prominence as alternatives to metallic housings due to their excellent specific mechanical properties, manufacturing flexibility, and flame-retardant formulations, enabling significant weight reduction and by extension enhanced vehicle efficiency and range.

Despite these advantages, the performance of polymer composites remains highly sensitive to environmental factors, with moisture absorption being among the most critical. Water ingress alters the resin microstructure through swelling and plasticization, weakens fiber–matrix interfaces, and can induce microcracking, all of which degrade stiffness, strength, and energy absorption capability. Moisture absorption in polymer matrix composites is primarily governed by diffusion processes that are commonly described by Fick's second law [1,2]. Water molecules penetrate the polymer matrix through a combination of molecular diffusion and capillary transport along fiber-matrix interfaces and microvoids [2,3]. At early exposure times, the absorption rate increases proportionally to the square root of time, followed by a saturation plateau as equilibrium is approached. Although many polymers follow ideal Fickian diffusion, numerous deviations have been reported due to morphological relaxation, hydrolysis, or microcracking within the resin network [4,5]. Such non-Fickian behavior arises from both physical and chemical changes that alter the effective diffusion coefficient during exposure [6–8]. In reinforced composites, fiber architecture plays a crucial role in moisture transport and resulting

* Corresponding author.
*E-mail address:* kitserpes@upatras.gr (K. Tserpes).

https://doi.org/10.1016/j.compositesb.2025.113349
Received 8 October 2025; Received in revised form 17 December 2025; Accepted 23 December 2025
Available online 24 December 2025

damage mechanisms. While glass and carbon fibers are largely impermeable, the fiber-matrix interface often serves as a preferential path for moisture ingress [3,8]. Shen and Springer [9] demonstrated that the diffusion coefficients in the fiber-parallel ($D_{11}$) and transverse ($D_{22}$) directions differ substantially, resulting in anisotropic diffusion behavior. However, in thick or plate-like geometries, such as those of battery housings, the through-the-thickness diffusivity ($D_z$) dominates the overall moisture uptake when the specimen's aspect ratio exceeds 100. This behavior has been validated in experimental and numerical studies of flax and glass fiber composites, confirming that the moisture transport is largely controlled by the thickness dimension [10]. To account for these effects, corrections for edge diffusion have been developed, allowing more accurate estimation of anisotropic diffusion constants using the Shen–Springer formulation [4,5,9,11].

The extent of moisture absorption is also strongly influenced by the matrix chemistry. Thermoset matrices have been the state-of-the-art choice compared to thermoplastics, due to their easier fiber impregnation, lower processing temperatures and cost [12]. However, at the same time, thermoplastic matrices, such as Elium®, typically exhibit lower equilibrium moisture content compared to thermoset epoxies [13–16]. Davies and Arhant [17,18] reported equilibrium moisture contents of approximately 0.4 % for glass/Elium® composites versus 1.2 % for glass/epoxy systems, while Chilali et al. [10,19] observed similar trends in flax fiber composites, attributed to the resin's low polarity and amorphous microstructure, which restricts the formation of hydrogen-bonding sites [15,20]. Beyond reduced hygroscopicity, the thermoplastic nature of Elium® is suited for both Vacuum-Assisted Resin Infusion (VARI), Resin Transfer Molding (RTM), as well as SMC processes and provides recyclability, enhanced toughness and damage tolerance compared to conventional thermoset matrices, which are particularly relevant for impact dominated loading conditions in battery housing applications [21]. Nonetheless, even in these systems, prolonged immersion can induce microstructural changes that lead to irreversible damage such as interfacial decohesion, microcracking, and local stress redistribution when internal osmotic pressures exceed the matrix strength [11,22]. Multi-scale damage analyses by Shirinbayan et al. [23] on advanced sheet molding compounds (A-SMC) highlight that even under different loading modes - tension, compression, and shear loading - the predominant failure mechanism remains the interfacial debonding between the fiber and the matrix. Penavayre et al. [24], noted that moisture absorption in carbon fiber-reinforced polyphthalamide (CF/PPA) can lead to significant physicochemical changes, interfacial degradation [25] and a notable reduction in glass transition temperature ($T_g$), confirming matrix plasticization.

In addition to the matrix and fiber effects, the inclusion of inorganic fillers further modifies the composite's moisture response. Aluminum hydroxide (ATH), commonly used as a flame-retardant and thermal stabilizer [26,27], influences both the mechanical and diffusion behavior of thermoplastic systems. While ATH itself is insoluble in water [28], residual stresses around filler particles act as stress concentrators that promote localized moisture ingress [7], due to the mismatch in thermal expansion between filler and resin generating regions of elevated stress. At the same time, though, the presence of ATH reduces overall hygroscopicity of a polymer composite. In Elium-based systems, the low initial viscosity and room temperature polymerization of the acrylic resin facilitate homogeneous dispersion and high loadings of ATH, while limiting residual stresses associated with processing [15,21], compared to thermoset composites. Studies on polymethacrylic-based Elium® composites have also demonstrated that ATH enhances the thermal stability of the matrix and mitigates shrinkage during high-temperature processing [29], making the prediction of moisture-related degradation in filled thermoplastic systems particularly challenging [30].

The mechanical implications of moisture absorption are equally significant, as they lead to a decrease in elastic modulus and strength [15,26,27,31–33]. These transformations have critical consequences under dynamic loading, as the impact energy absorption mechanism depends strongly on stiffness and integrity of the matrix-fiber interface.

Although the diffusion and mechanical degradation of thermoset composites have been widely studied, a significant research gap remains regarding thermoplastic SMCs. Specifically, no prior study has coupled three-dimensional moisture diffusion, moisture-dependent property degradation, and full scale impact performance for these materials. The present work addresses this gap by experimentally and numerically examining the moisture absorption process of an Elium®, glass fiber, $Al(OH)_3$ sheet molding compound system and its subsequent influence on the crashworthiness of a battery housing. Immersion experiments were conducted according to ASTM D570 and D5229, allowing determination of the 3D diffusion coefficients and equilibrium moisture content for different conditioning durations (0, 1000, 2000, and 3000 h). The experimentally measured mechanical property degradations were incorporated into validated finite-element (FE) models to simulate low- and medium-velocity impacts from 10 m/s to 25 m/s. The novelty of this work lies in its integrated treatment of hygrothermal aging, mechanical property evolution, and impact simulation in a complex SMC thermoplastic system. By establishing an association between environmental conditioning and crashworthiness, the study contributes new insights into the design of durable, lightweight, and recyclable composite enclosures for next-generation electric vehicles.

## 2. Experimental

### 2.1. Material

The composite material is comprised of a thermoplastic matrix, that consists of Arkema Elium MC 590 acrylic resin enhanced with 63 wt % aluminum hydroxide, Martinal ATH. $Al(OH)_3$ is an environmentally friendly metallic hydroxide flame retardant, which improves the composite's thermal stability, especially at higher filler contents [26,27,34]. For mechanical strength and stiffness, the matrix is reinforced with 20 wt % chopped glass fibers (JM Multistar 272). The housing has maximum external dimensions of 440 mm × 300 mm × 89 mm and a wall thickness varying between 3.0 and 3.5 mm, due to its manufacturing process. The material is processed as a Sheet Molding Compound (SMC), a prepreg format designed for compression molding. All stages of production, from semi-finished SMC sheet formulation to compression molding of flat panels and the housing component, were performed at Fraunhofer ICT in Pfinztal, Germany [35].

### 2.2. Moisture absorption test

Moisture absorption testing is conducted following the ASTM D570 and ASTM D5229 standards, to evaluate the relative rate of absorption when a plastic composite is immersed in water [36,37]. Two types of flat, rectangular specimens (250 mm × 25 mm × 2.5 mm and 95 mm × 18 mm × 4.5 mm) are conditioned in deionized water, for 3000 h. Prior to immersion, the specimens were conditioned in an oven at 50°C for a day to release any moisture from the environment and then were weighed, using an analytical balance capable of 0.1 mg accuracy, measuring the initial mass $W_o$. After that, the specimen's mass was monitored every day for the first 48 h, after seven days (168 h) and every two weeks until saturation was reached. Measurements were also taken at 1000, 2000 and 3000 h of conditioning, to correlate with mechanical testing of tension and three-point bending.

The average amount of moisture absorbed in the material was expressed as a percentage, as follows by Eq. (1):

$$M = \frac{W_i - W_o}{W_o} \times 100 \tag{1}$$

where $W_i$ is the current specimen mass and $W_o$ is the oven-dry specimen mass.

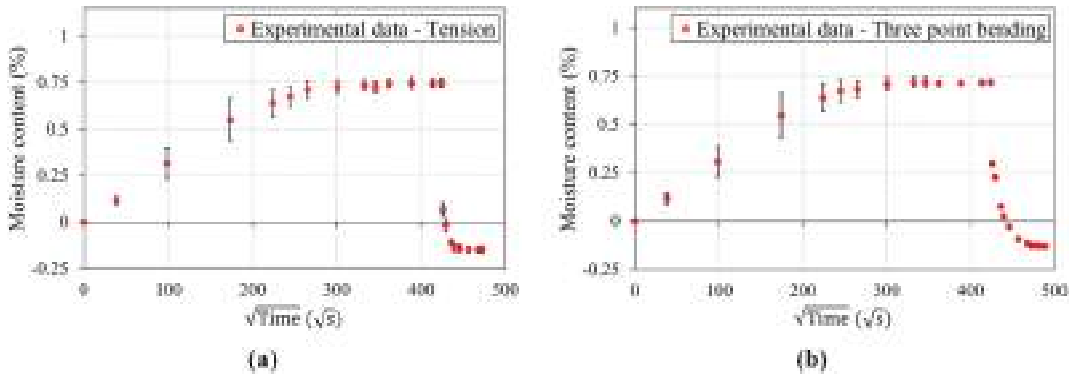


**Fig. 1.** Moisture absorption and desorption vs time curves for the (a) tension, (b) three-point bending specimens.

In order to determine if the specimen has reached saturation, the effective moisture equilibrium content is determined. Moisture equilibrium can be either absolute or effective, with absolute meaning no measurable change in the moisture content, whereas effective allows a specified small change in the average content over the reference time period. The specimen can be defined in saturation state when the average moisture content of the material changes by less than 0.020 % between two consecutive reference time period spans.

For the desorption process the same principle is followed, where the weight at saturation state is taken as a baseline mass and the specimens are dried in an oven, located in a room with standard laboratory atmosphere, at 50°C. Weighing the specimens occurred after 24 and 48 h of heating and then after five days. After that, measurements were taken every five days, till equilibrium was reached and no more moisture was released. Using Eq. (1), the percentage of lost mass was calculated, where, in this case, $W_i$ is the oven-dry specimen mass and $W_o$ the absorption baseline specimen mass.

In order to measure the material's resistance to water ingress, the diffusion coefficient is calculated by Eq. (2), following Fick's one dimensional law, in the through-the-thickness direction:

$$D_z = \pi\left(\frac{h}{4M_m}\right)^2\left(\frac{M_2 - M_1}{\sqrt{t_2} - \sqrt{t_1}}\right)^2 \tag{2}$$

where h is the average specimen thickness, $M_m$ the effective moisture equilibrium content, and $\frac{M_2-M_1}{\sqrt{t_2}-\sqrt{t_1}}$ the slope of moisture absorption plot in the initial linear portion of the curve.

When investigating moisture diffusion in composites, it is necessary to use infinite thin specimens to ensure that the process is governed by one-dimensional diffusion. However, since finite plates are used in an experiment, moisture diffuses through all six faces. This implies the observed weight change is the sum of diffusion in all three directions, and the experimentally determined diffusion coefficients are affected by the specimen's dimensions [38]. According to ASTM standards and Springer's theory, an aspect ratio of length-to-thickness (l/h) greater than 100 is recommended to minimize edge effects [2,36,37]. This ensures that the diffusion is primarily governed by thickness, allowing the material to reach saturation in a predictable way.

In this study, specimens were cut according to standard dimensions for mechanical testing. One specimen type follows the 100:1 aspect ratio, so the one-dimensional approximation can be implemented. In this case, edge effects are minimized but should still be accounted for, by implementing in the calculation a correction derived by Shen and Springer [39]. The true one-dimensional diffusion coefficient $D_z$ can be calculated by Eq. (3):

$$D_z = ED_a = D_a\left(1 + \frac{h}{l} + \frac{h}{w}\right)^{-2} \tag{3}$$

where $D_a$ is the apparent diffusion coefficient, calculated from the test by Eq. (2) and E is the correction factor that is correlated with the specimen's dimensions.

The second type of specimen used in this study deviates from the recommended aspect ratio, suggesting that there may be a greater flux through the edges than the thickness direction. Anisotropic moisture diffusion is considered, with different coefficients in the three directions. In this case, calculations from Eq. (2) will result in $D_a$, and the diffusivity coefficients $D_x$, $D_y$, $D_z$ along the length, across the width and through the thickness of the material, are given by the following relationship, Eq. (4):

$$D_a = D_z\left(1 + \frac{h}{l}\sqrt{\frac{D_x}{D_z}} + \frac{h}{w}\sqrt{\frac{D_y}{D_z}}\right)^2 \tag{4}$$

Assuming $D_x = D_y$, due to the transversely isotropic behaviour of the short fiber composite, the diffusivity coefficient is given by Eq. (5):

$$\sqrt{D_a} = \left(\frac{h}{l} + \frac{h}{w}\right)\sqrt{D_x} + \sqrt{D_z} \tag{5}$$

Due to uncertainties in measurement instruments, testing procedures, and sample-to-sample variation, an estimation of the uncertainties of the calculations was necessary. Following the methods outlined in UKAS M30003, a normal distribution was assumed for these calculations, which implies using a coverage factor of 2 [1,39].

The uncertainty of the edge correction factor can be calculated as:

$$\Delta E^2 = 2\left[\left[\left(\frac{\Delta h}{h}\right)^2 + \left(\frac{\Delta l}{l}\right)^2\right]\left(\frac{l}{h}\right)^2 + \left[\left(\frac{\Delta h}{h}\right)^2 + \left(\frac{\Delta w}{w}\right)^2\right]\left(\frac{h}{w}\right)^2\right] \tag{6}$$

And the uncertainty of the diffusion coefficient, is given by the following equation:

$$\left(\frac{\Delta D_a}{D_a}\right)^2 = 2\left[\left(\frac{\Delta h}{h}\right)^2 + \left(\frac{\Delta C_s}{C_s}\right)^2 + \left(\frac{\Delta C_{t2} - \Delta C_{t1}}{C_{t2} - C_{t1}}\right)^2 + 0.5\left(\frac{\Delta t_2}{t_2}\right)^2\right] \tag{7}$$

where $C_s$ the concentration at saturation, $C_{t1}$ is the concentration at the dry state, at time $t_1$, which is taken as zero, and $C_{t2}$ is the concentration at the end of the linear diffusion at time $t_2$.

### 2.2.1. *Moisture absorption/desorption behaviour*

The percentage of absorbed moisture, according to Eq. (1), that corresponds to each weighting, is plotted with time. Fig. 1 shows the moisture absorption rate for the two types of specimens. Overall, the two curves have a similar behaviour, confirming consistency of the material's properties regardless of the different aspect ratios. The specimens cut for tension tests, had greater length and width, but smaller thickness, whereas the specimens destined for three point bending tests had a smaller length and width, but were thicker. The larger surface resulted in a greater percentage of absorbed moisture for the tension specimens,

**Table 1**
Diffusion coefficients and uncertainty of correction factors and apparent diffusivity percentage.

| Property | Value | |
|---|---|---|
| | Thin specimens (aspect ratio: 100) | Thick specimens (aspect ratio: 21) |
| Apparent diffusivity coefficient, $D_a$ | $2.100 \times 10^{-5}$ $mm^2/s$ | $5.448 \times 10^{-5}$ $mm^2/s$ |
| Diffusivity coefficient along the length, $D_x$ | $1.713 \times 10^{-5}$ $mm^2/s$ | $2.877 \times 10^{-5}$ $mm^2/s$ |
| Diffusivity coefficient across the width, $D_y$ | $1.713 \times 10^{-5}$ $mm^2/s$ | $2.877 \times 10^{-5}$ $mm^2/s$ |
| Diffusivity coefficient through the thickness, $D_z$ | $1.713 \times 10^{-5}$ $mm^2/s$ | $3.322 \times 10^{-5}$ $mm^2/s$ |
| Uncertainty of edge correction factor, $\Delta E$ | 0.446 % | 0.197 % |
| Uncertainty of the diffusion coefficient, $\Delta D_a/D_a$ | 17.106 % | 12.098 % |

of 0.748 ± 0.023 %, compared to 0.718 ± 0.011 % for the three-point bending specimens.

The absorption curves show a rapid increase in moisture content for the first 1000 h, which then reaches a plateau for the remaining 2000 h, indicating the material's saturation. The long term immersion of 3000 h enabled deep understanding of the absorption mechanisms of the chopped fiber thermoplastic composite. For the first 2000 h, the moisture uptake aligns with Fickian behavior. This is where the most significant variation in the measurements was observed, where deviation was calculated between ±0.083 and ± 0.115 percentage of moisture uptake. Some discrepancies in moisture uptake can be attributed to variation in the chopped fiber distribution within each specimen. Samples with a higher percentage of fibers tend to show lower percentage of moisture absorption, while those with a greater percentage of resin material display higher absorption rates. However, these differences are normalized once the material reaches its saturation point.

After the initial Fickian phase, small variations in moisture content at 2000 h suggest a shift to non-Fickian behavior. A small decrease in the moisture content is observed at first, that can be attributed to potential dilution of the resin in deionized water, which penetrates the polymer macromolecules increasing the mobility of the molecular chains [6]. The subsequent increase is due to penetration of additional moisture in defects and cavities that have been created because of the matrix reduction. Usually, changes in the microscopic structure of polymer composites lead to anomalous diffusion. These changes are induced by swelling and plasticization of the matrix, namely hydrophilization which increases the equilibrium water uptake [30], debonding on the fiber-matrix interface and matrix defects that have been created during processing, such as voids and microcracks [2]. At prolonged moisture exposure, these microcracks propagate, causing irreversible internal damage to the composite [11].

This phenomenon was consistently observed across all SMC specimens, since the standard deviation that was calculated was less than 0.012 %, ensuring consistency and reliability of the material's behaviour. After these fluctuations, the moisture content reaches a second plateau which is maintained until the 3000-h point of conditioning.

After 3000 h of water immersion, the specimens were conditioned in a dry atmosphere and were heated at 50°C until they reached a desorption equilibrium. The thinner specimens (tension) in Fig. 1(a) release moisture much faster than the thicker specimens, in Fig. 1(b). This results in 750 and 1000 h of conditioning until the tension and three-point bending specimens reach a clear plateau, respectively. It should be remarked that the specimens' mass after desorption was lower than their initial dry mass, calculated before water immersion. More specifically, the mass of the tension specimens after desorption is 0.147 % lower than its initial dry state, and for the three-point bending specimen it is decreased by 0.129 %.

The measured mass loss following desorption cannot be directly partitioned among individual degradation mechanisms. It can be attributed to the non-Fickian behavior observed during immersion and the solubility of the composite's components, as well as its dehydration during desorption, due to thermal processing. The use of deionized water, which creates higher osmotic pressure due to its low mineral content, can accelerate this process [22].

This composite is comprised of three critical elements, the glass fibers, and the matrix that contains both ATH particles and the Elium resin. Glass fibers are insoluble to water and present very low absorption behaviour [1,5]. What can interact with water is the sizing of the fibers, which in the present case is saline based. The contribution of saline-based glass fiber sizing to moisture uptake was not experimentally isolated and is inferred from published studies indicating its hydrophobic nature [40,41].

Therefore, mass loss due to solubility and dehydration of the composite is primarily linked to the matrix components. The use of micro sized Alumina Trihydrate (ATH) as the additive in the formulations intends to reduce the hygroscopic tendency of the composites [34]. The hydrolysis of ATH is pH dependent. In neutral pH, between 6 and 7, ATH is essentially insoluble and remains stable solid, while in slightly acidic pH, lower than 6, ATH can showcase partial dissolution [28]. The possibility of significant degradation of the filler is more prominent in elevated temperatures, which can result in dehydration of the ATH particles that cause mass loss [29]. In the present study, no thermal or spectroscopic analyses were conducted, and the pH of the deionized water was not monitored during the immersion tests. However, although deionized water may drift toward mildly acidic values due to atmospheric $CO_2$ absorption, the low conditioning temperature (50 °C), ensuring that thermal exposure remained within the glassy state [24,25], and the exposure conditions suggest limited chemical interaction with the ATH filler.

Instead, the observed mass loss is primarily attributed to phenomena related to the polymer's nature. With regards to the thermoplastic resin, Elium is considered insoluble in water. However, although it might not break down chemically, long term water immersion can first lead to swelling, while the water molecules infiltrate the polymer, and then dissolve due to chain unzipping, namely the untangling of the polymer chain [20]. In higher temperatures, Elium matrix can undergo thermolysis, which again causes unzipping, and thermal oxidization, that leads to matrix degradation and mass loss [20,29].

### 2.2.2. *Diffusivity coefficients and uncertainty*

The moisture absorption curve, shown in Fig. 1, was used to determine the initial linear incline, which corresponds to the apparent diffusivity constant. For the thin, tension specimens, linearity is preserved for the first 750 h of conditioning, whereas for the thick, three-point bending specimens the curve is linear until 1000 h. The apparent diffusivity constants are calculated in the through-the-thickness direction by Eq. (1), 2.100 × 10-5 $mm^2/s$ and 5.448 × 10-5 $mm^2/s$, respectively for the thin and thick specimens. Edge effects were accounted for using a correction factor, allowing for the determination of the through-thickness diffusivity constant, $D_z$, and $D_x = D_y$ are calculated by solving Eq. (5), for the different dimensions of each specimen type.

While thin specimens have a shorter through-thickness pathway, they exhibit a lower apparent diffusivity compared to thick specimens due to the influence of their geometry. In longer and thin specimens, a significant amount of moisture enters through the side faces, that cover a greater surface. This way, moisture travels along the fiber-matrix interfaces, which often acts as barriers that hinters the diffusion process, resulting in a lower apparent diffusivity. On the contrary, in short, thick specimens, moisture transport is predominantly governed by direct, through the thickness pathway, which is shorter and less influenced by the resistive interfaces. This direct penetration leads to a faster saturation rate and, consequently, a higher apparent diffusivity [42].

**Table 2**
Mechanical properties of the SMC material for different conditioning times.

| Property | Value | | | | |
|---|---|---|---|---|---|
| | Absorption | | | | Desorption |
| | 0 h | 1000 h | 2000 h | 3000 h | 750/1000 h |
| Tensile strength, MPa | 94.99 | 57.42 | 45.97 | 44.49 | 51.84 |
| Modulus of Elasticity, GPa | 12.26 | 9.15 | 8.03 | 8.02 | 13.46 |
| Flexural strength, MPa | 190.31 | 93.54 | 85.42 | 85.83 | 99.92 |
| Flexural modulus, GPa | 12.91 | 7.88 | 7.87 | 7.80 | 13.42 |

The uncertainty of the edge correction factor, accounts for deviations in the specimen dimensions, especially the thickness. In this study, the tension specimens average measured dimensions included a length of 250 ± 0.500 mm, width of 24.779 ± 0.277 mm and thickness of 2.417 ± 0.072 mm. Similarly, the three-point bending specimens measured, 95 ± 0.332 mm in length, 17.994 ± 0.058 mm in width and 4.561 ± 0.011 mm thickness. These small standard deviations resulted in a very low percentage of uncertainty for the edge correction factors of 0.446 % and 0.197 %, for the thin and thick specimens, as described in Table 1.

Regarding the calculation of the uncertainty of the diffusion coefficients, Eq. (7) was employed. Although $C_{t1}$ was taken to be zero, a standard deviation of ±0.072 and ± 0.056 was assumed, the same as the standard deviation in the saturation value for the tension and the three-point bending specimen, respectively. This was included to account for potential variability in the dry state that could be caused by insufficient drying or potential moisture absorption from the atmosphere before the first weighing. The calculations resulted in an uncertainty of 17.106 % for the thin specimens and 12.098 % for the thicker specimens, concerning the experimental calculation of the diffusivity coefficient, while assuming normal distribution and a coverage factor of 2. An uncertainty under 20 % is considered acceptable for diffusivity measurements in fiber-reinforced composites, since such systems showcase strong microstructural heterogeneity, influenced by fiber distribution and orientation, interfacial bonding, and porosity, factors that introduce a high level of variability that is difficult to completely control or capture through experimentation [43].

### 2.3. Mechanical testing

In order to evaluate the degradation of mechanical properties of the composite, at different stages of water absorption, standardized tension and three-point bending tests were performed. The tests were conducted after 0, 1000, 2000 and 3000 h of conditioning in deionized water, for the absorption process and after 750 and 1000 h of conditioning at 50°C, for the desorption process.

For each test, at least five specimens were prepared and tested under controlled conditions of 23 °C and 50 % relative humidity and all tests were conducted on a 100 kN MTS Universal Testing Machine with hydraulic grips. Consistent with the material's randomly oriented short glass fibers, the specimens were tested without end tabs, as permitted by the applicable ASTM standards [44].

Tensile properties were evaluated using the ASTM D3039 standard. Flat, rectangular specimens measuring 250 mm × 25 mm × 2.5 mm were subjected to tensile loading at a crosshead speed of 1 mm/min. These measurements were used to calculate the tensile modulus of elasticity, in addition to determining the ultimate tensile strength of the material.

The flexural strength and flexural modulus were measured using a three-point bending configuration, following ASTM D790. The specimens measured 95 mm × 18 mm × 4.5 mm and were tested with a support span-to-depth ratio of (16 ± 1):1 at a crosshead speed of 2.2 mm/min.

#### 2.3.1. Mechanical tests after moisture absorption and desorption

Table 2 summarizes the properties derived from tension and three-point bending testing. During the absorption process, the material properties deteriorate exponentially with time and remain relatively stable when the material reaches saturation, between 1000 and 3000 h of water conditioning. The desorption process results in partial recovery of the material's strength, in both tensile and flexural tests, and even a small increase in the tensile and flexural modulus. A major decrease in properties is observed between the dry specimens and the first 1000-h

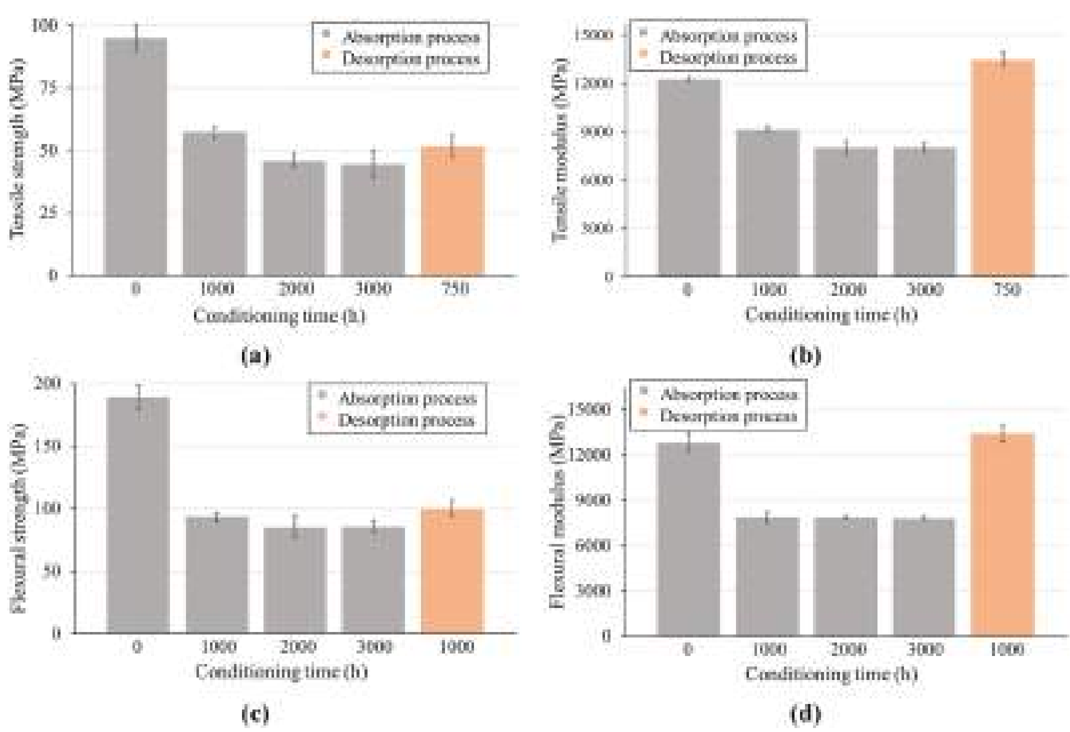


**Fig. 2.** Comparison of the tensile (a) strength, (b) modulus and the flexural (c) strength, (d) modulus for different conditioning times.

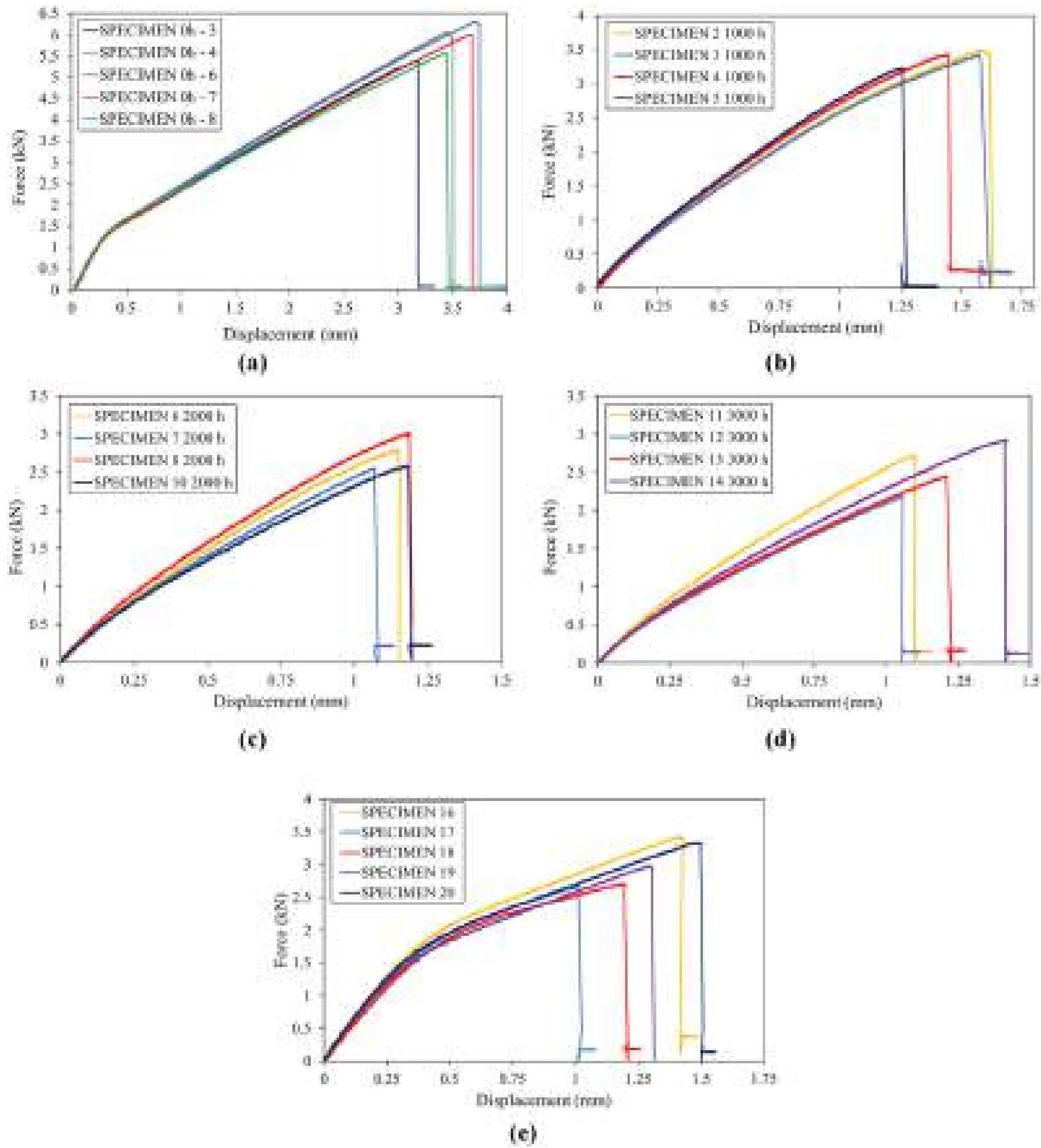


**Fig. 3.** Force-displacement curves for the tension test at (a) 0, (b) 1000, (c) 2000, (d) 3000 h of immersion in water and (e) 750 h of conditioning at 50°C (desorption).

conditioned ones, with tensile and flexural strengths, declining by 39.55 % and 50.84 %, respectively. At 3000 h, when saturation has fully occurred, the final deterioration of the strengths is 53.16 % and 54.89 % for tension and three-point bending. The tensile modulus decreases after 1000 h by 25.36 % and by 34.58 %, after 3000 h of immersion. Similarly, the flexural modulus is reduced by 38.96 % and 39.58 %, after 1000 and 3000 h, respectively.

After desorption, an increase of 16.52 % and 16.41 % is observed for the tensile and flexural strength, compared to the properties at saturation state, which indicates that after thermal treatment and moisture removal, part of the mechanical strength is recovered. Conditioning at 50°C improved the tensile and flexural modulus by 9.78 % and 3.95 % compared to the properties of the dry specimens, respectively. This indicates that thermal treatment changes the microstructure of the composite, which makes the material behave in a stiffer manner.

Fig. 2 shows the standard deviation resulting from each test, which ranges from 1.17 % to 4.93 % for the tensile modulus, 1.52 %–4.83 % for the flexural modulus. Tensile strength values varied from 3.64 % to 11.88 %, and flexural strength from 4.04 % to 10.15 %. Results above the acceptable limit of 10 % variation were observed at 2000 h of water conditioning, in the flexural strength, which shows a variation of 10.15 %, and in tensile strength at 3000 h of conditioning with 11.88 % variation. Overall, testing showed a small percentage of variation, with the two properties mentioned deviating probably due to different absorption rates at the time of testing, that affected the degree of the matrix deterioration and the fiber-matrix interface debonding, resulting in minor scattering of the mechanical properties.

Moisture absorption in composite materials is mainly defined by three mechanisms - swelling, plasticization, and chemical degradation [16]. Swelling occurs when liquid molecules are absorbed into the polymer matrix, causing a volume expansion that alters the composite's, essentially the matrix's, residual stress state. This process leads to irreversible damage, mainly fiber-matrix debonding and microcracks, that occur due to the anisotropic distribution of absorbed liquid and the difference in swelling behavior between the matrix and the fibers, that are predominantly hydrophobic. At the same time, plasticization takes place as liquid molecules replace the intermolecular bonds, namely the hydrogen bonds, between polymer chains, which increases free volumes in the composite microstructure, enabling easier chain movement. This effect reduces stiffness and strength, as it contributes to interface failure

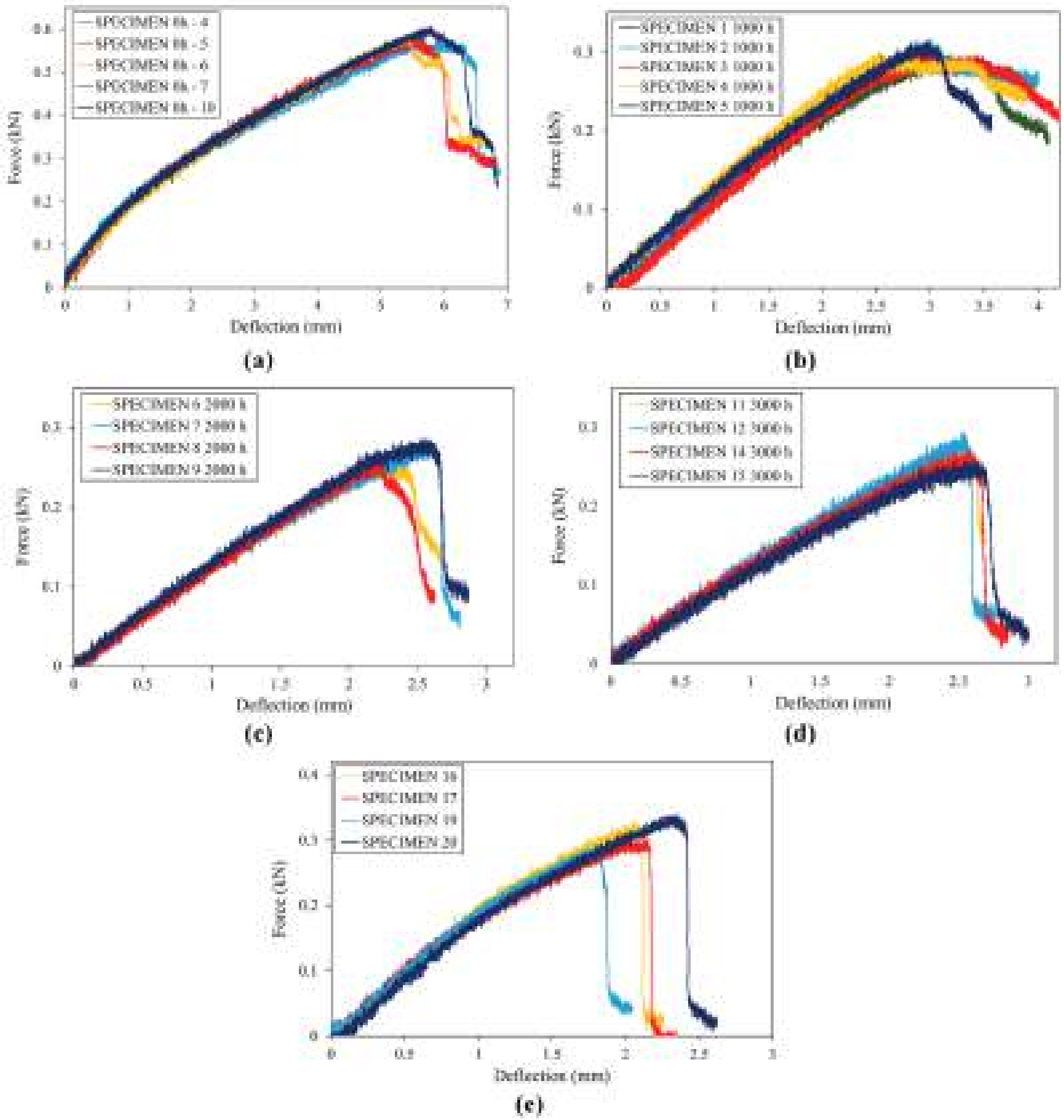


**Fig. 4.** Force-deflection curves for the three-point bending test at (a) 0, (b) 1000, (c) 2000, (d) 3000 h of immersion in water and (e) 1000 h of conditioning at 50°C (desorption).

and void expansion. However, it can be reversible when moisture is removed from the material. Chemical degradation involves hydrolysis of bonds at the fiber-matrix interface and oxidation of unsaturated bonds within the resin, causing further degradation of the composite's mechanical properties [3,45,46].

The force-displacement response of the specimens subjected to tensile loading is presented in Fig. 3 for different conditioning times, from the dry state until saturation at desorption. Before water immersion, the material shows bilinear behaviour that is attributed to the aluminum hydroxide additive, which improves the mechanical properties of the composite. However, a high amount of ATH filler contributes to more voids and pores in the material, that interferes with the interface quality between the matrix and the fibers [27,34]. The initial linear area corresponds to the elastic modulus (12.26 GPa) and is significantly greater than the tangent modulus (3.68 GPa), which represents the second linear area. This can be attributed to the fact that after initial loading, which represents aluminum hydroxide reinforcement, the decohesion between matrix and reinforcement becomes more dominant, resulting in a stiffness closer to the one of the Elium resin. During the first 1000 h of conditioning, a major degradation can be observed between Fig. 3(a) and (b). The ultimate tensile load has dropped almost in half, as well as the ultimate displacement. At the same time, the material shows more brittle behaviour, without a very noticeable bilinear area, indicating matrix degradation. Fig. 3(c) and (d), reveal a comparable behaviour between degradation at 1000 h and 2000 and 3000 h of water conditioning. The rapid degradation observed in the initial phase of moisture absorption can be attributed to the Fickian diffusion process, which induces fiber-matrix interface debonding through swelling. After this, the slower degradation corresponds to a non-Fickian diffusion process dominated by polymer relaxation. The combination of these mechanisms can significantly reduce the service reliability of these composite structures, resulting in premature failure. While matrix plasticization can initially lead to a more ductile, shear-yielding failure, the decrease in matrix yield strength can cause brittle failure, where a crack initiates perpendicular to the fiber. This phenomenon is reinforced by decreased displacement at failure, due to fiber breakage or matrix degradation. In most force-displacement curves, a varying displacement at failure is observed, which can be associated with the composite's heterogeneity, particularly due to the randomly oriented chopped fibers that affect the ultimate strain capacity of individual specimens within the same test batch.

During moisture absorption, the polymer matrix undergoes plasticization, which increases the free volumes and chain mobility in the composite. This phenomenon reduces the material's bilinear behaviour, making the force-displacement curve appear more linear, with a less distinct yield point. However, during the desorption process, the absorbed water molecules are removed, enabling the polymer and their intermolecular bonds to reform [3,47]. This allows the matrix to return to a state closer to its unconditioned form, which is illustrated in Fig. 3(e), where the force-displacement curve after desorption exhibits again bilinear behavior. Despite that, the damage from moisture absorption cannot be fully reversed. While the matrix regains its stiffness, moisture-induced swelling has caused permanent changes at the composite's microstructure, with micro-cracks and interface debonding. Therefore, even though the matrix's bilinear behavior appears, the composite's overall mechanical performance remains compromised, which is established by the reduced strength and displacement at failure.

Regarding the three-point bending results, the composite in its dry state, as illustrated by the force-displacement curve in Fig. 4(a), exhibits high flexural strength, indicating effective interfacial bonding between the matrix and the reinforcing fibers [12]. The performance of the material deteriorates significantly in the time period between 0 and 1000 h (Fig. 4(b)) of water immersion but the phenomenon does not escalate in the next two 1000-h testing intervals, as depicted in Fig. 4(c) and (d). This can be attributed to the fact that flexural properties are mainly affected by the matrix material. When saturation has been reached, after 1000 h, the matrix does not notably degrade, resulting in similar behaviour even after prolonged water conditioning. After desorption, moisture removal reassigned some matrix characteristics concerning the ductility and stiffness of the composite, but did not substantially change its reduced performance in strength and displacement at failure, following saturation. Essentially, the exposure to moisture and the subsequent drying process at elevated temperature, acted as an additional conditioning step that permanently altered the composite's microstructure [14], leading to a higher elastic modulus after desorption compared to the initial dry state. This effect can be attributed to the fact that heat exposure promotes post-curing of the polymer chains, creating new chemical bonds that permanently increase the stiffness of the matrix, while also, altering the interaction between the matrix and aluminum hydroxide that may have led to a more effective load transfer, thus improving the elastic modulus.

## 3. Analytical models

Several models have been developed to characterize the diffusion of water molecules within composite materials [10,38,48]. Fick's second law is commonly used as a fundamental tool to describe both the one- and three-dimensional, time-dependent process of moisture absorption.

### 3.1. One dimensional Fick's law of diffusion

Fick's law differential equation is defined by:

$$\frac{\partial C}{\partial t} = div\left(D\cdot\overrightarrow{grad}C\right) \tag{8}$$

where C is the moisture concentration and D is the symmetric diffusion tensor.

Considering an infinitely thin plate, Fick's second law is used to describe one-dimensional diffusion in the through-the-thickness (z) direction by:

$$\frac{\partial C}{\partial t} = D_z\frac{\partial^2 c}{\partial z^2} \tag{9}$$

where C is the moisture concentration in the material, $D_z$ is the constant diffusion coefficient in the through-the-thickness direction, t is the time, and z is the location in the through-the-thickness direction of the material.

For the moisture absorption process in an initially dry thin plate with thickness h and z = 0 representing the central plane with surfaces at z = $\pm$ h/2, the initial and boundary conditions of C (z, t) can be expressed as:

$$\begin{gathered} C(z,0) = 0, \text{for} |z| < \frac{h}{2} \\ C\left(-\frac{h}{2},t\right) = C\left(\frac{h}{2},t\right) = C_\infty, \text{for all t} \end{gathered} \tag{10}$$

where $C_\infty$ is the equilibrium moisture concentration.

By solving Eq. (9) with the initial and boundary conditions of Eq. (10), namely considering uniform initial distribution and equal initial surface concentration, the moisture uptake M(t), in one dimension, can be calculated by:

$$\frac{M_t}{M_\infty} = 1 - \sum_{n=0}^{\infty}\frac{8}{(2n-1)^2\pi^2}\exp\left(-\left(\frac{D(2n+1)^2\pi^2 t}{4l^2}\right)\right) \tag{11}$$

where $M_t$ denotes the total amount of moisture entering the material at time t, $M_\infty$ denotes the moisture content after infinite time, at saturation, D is the diffusivity constant, and l denotes the half thickness of the plate.

### 3.2. Three dimensional Fick's law of diffusion

Based on Eq. (8), Fick's law for an anisotropic material is described by the following equation:

$$\frac{\partial C}{\partial t} = D_{xx}\frac{\partial^2 c}{\partial x^2} + D_{yy}\frac{\partial^2 c}{\partial y^2} + D_{zz}\frac{\partial^2 c}{\partial z^2} + 2D_{xy}\frac{\partial^2 c}{\partial x\partial y} + 2D_{xz}\frac{\partial^2 c}{\partial x\partial z} + 2D_{yz}\frac{\partial^2 c}{\partial y\partial z} \tag{12}$$

where $D_{xx}$, $D_{yy}$ and $D_{zz}$ are the moisture diffusivity constants in the x, y and z directions, respectively, and $D_{xy}$, $D_{xz}$ and $D_{yz}$ represent the moisture diffusivity in the x, y, z directions due to a moisture concentration gradient in the x, y, z directions, accordingly.

When the material principal directions (1, 2, 3) coincide with the reference directions (x, y, z), Fick's law becomes:

$$\frac{\partial C}{\partial t} = D_1\frac{\partial^2 c}{\partial x^2} + D_2\frac{\partial^2 c}{\partial y^2} + D_3\frac{\partial^2 c}{\partial z^2} \tag{13}$$

where $D_1$, $D_2$, $D_3$ are the principal moisture diffusion constants.

An analytical solution to Eq. (12) of the 3D Fick's law is calculated by:

$$\frac{M_t}{M_\infty} = 1 - \left(\frac{8}{\pi^2}\right)^3\sum_{i=0}^{\infty}\sum_{j=0}^{\infty}\sum_{k=0}^{\infty}\frac{exp\left(-\pi^2 t\left[\left(D_1\left(\frac{2i+1}{l}\right)^2 + D_2\left(\frac{2j+1}{w}\right)^2 + D_3\left(\frac{2k+1}{h}\right)^2\right)\right]\right)}{((2i+1)(2j+1)(2k+1))^2} \tag{14}$$

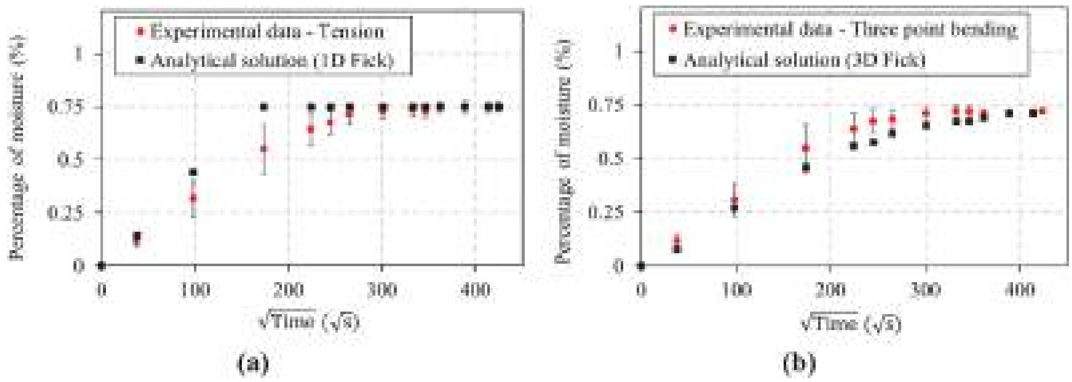


**Fig. 5.** Comparison of the experimental moisture absorption curves and the analytical solution of Fick's law for the (a) tension, (b) three-point bending specimens.

where l, w and h are the specimen's dimensions.

### 3.3. Property degradation model

Two models based on analytical solutions that predict the degradation of the composite's mechanical properties due to moisture absorption, will be used to provide predictive capability outside experimental observation. While testing reveals the degree of degradation at specific time points, an analytical model allows to extrapolate findings and predict the material's intermediate and long-term performance without having to conduct extensive experiments. In order to implement those models, it is important to assess the phenomenological causes of degradation and translate these phenomena to mathematical formulations. Most models are based on matrix and interface degradation [11, 19,49–53], since they are the most prominent factors for property deterioration during moisture absorption, and mainly focus on tensile and shear modulus determination. In this study, a linear and an exponential model will be implemented for the evaluation of both strength and elastic modulus in tensile and flexural testing, to compare with the respective experimental results.

#### 3.3.1. Linear model

During moisture absorption, water is transported from the external environment into the composite material. To correlate the moisture concentration, C, with the irreversible energy dissipation processes, such as damage to the fiber-matrix interfaces and resin degradation, an internal variable, a, is introduced. This variable is related to swelling and evolves from a value of 0 in the initial (t = 0), un-swollen state to a value of 1 at the equilibrium or the fully saturated state (at t∞). The internal variable can be measured using the following equation:

$$a = \frac{w_t}{w_\infty} \tag{15}$$

The internal variable, as defined in Eq. (15), is based on the maximum mass of absorbed water, $w_\infty$, and assumes that the amount of water stored in the composite's micro-voids is negligible, with this simplification allowing the variable to represent the extent of matrix swelling.

The theoretical prediction of property degradation can be derived by Eq. (16), where a linear relation between the property and the internal variable is implemented:

$$P_r = (1 - \beta\alpha)P_o \tag{16}$$

where $P_r$ is the current (residual) value of the mechanical property, $P_0$ is the value for the dry specimen and β is a positive constant defined as maximum degradation parameter (0<β < 1). When a = 0, $P_r$=$P_o$, verifying the initial boundary conditions of the equation, and when a = 1, $P_r = P_{sat}$ and β can be calculated as $(P_o - P_{sat})/P_o$.

#### 3.3.2. Exponential model

The second model is also concentrated on matrix degradation and is based on the mechanism of hydrolysis. This process involves water molecules invading the polymer chain, which results in the breakage of the polymer bonds. This chemical reaction significantly weakens the polymer's overall structure and leads to a reduction in the composite's mechanical properties. The exponential relation between the current mechanical property ($P_r$) and the initial mechanical property ($P_o$) is given by:

$$P_r = P_o \exp(-kW) \tag{17}$$

where W is the moisture concentration and k a fitting parameter that affects degradation.

### 3.4. Analytical results

#### 3.4.1. Experimental vs analytical moisture absorption curves

Comparing the moisture absorption curves for the thin (tension) and thick (three-point bending) specimens, with the analytical solutions derived from Eqs. (11) and (14), both graphs, in Fig. 5, show a strong agreement during the whole absorption process. This confirms that moisture uptake in this composite follows predominantly Fickian diffusion. The standard deviation is minimal in most experimental measurements, except for the weighting at 750 h of conditioning, which results in 20 % and 10 % variation from the theoretical values for the thin and thick specimens, as shown in Fig. 5(a) and (b), respectively. Overall, though, the deviation is insignificant and the overlapping error bars with the theoretical curves provide validation for the model's accuracy and a significant experimental repeatability. The observed differences between the one- and three-dimensional Fickian models with the experimental curves reinforce the calculated uncertainties of the diffusivity coefficient, namely the absorption rate, which were greater for the thinner specimens. Also, the analytical models, especially the one-dimensional one, predict a perfect saturation plateau, that corresponds well with the experimental data, which means that the models have demonstrated successful estimation in longer saturation times.

A higher value of diffusivity from the one-dimensional model for the thin specimens is due to its simplified assumption that moisture only diffuses through the thickness, neglecting diffusion along the side faces and fiber-matrix interfaces. The more complex 3D model, which accounts for diffusion from all six faces, provides a more accurate, although slightly lower, prediction of moisture absorption by including these pathways, that retard the diffusion process, reducing the overall apparent diffusivity and leading to a lower predicted value. The nature of the composite material, having randomly distributed chopped fibers, as well as the different aspect ratios, have resulted in a closer approximation of the diffusion process for the thick specimen, while for the thinner specimen, the simplifications resulted in a different diffusion rate.

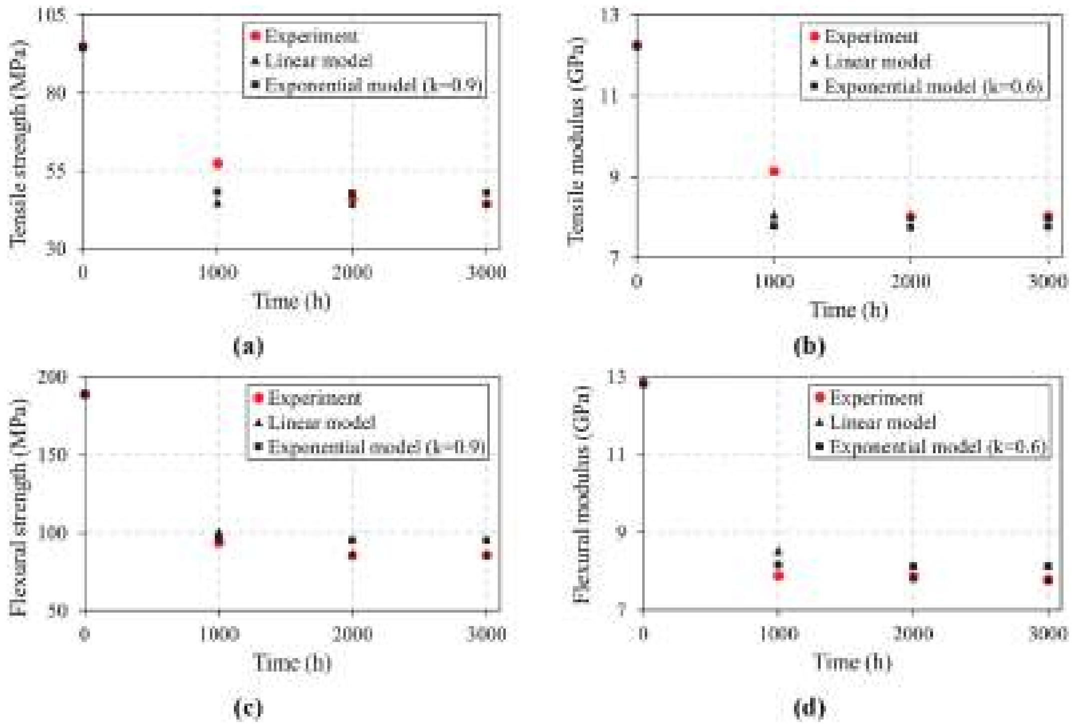


**Fig. 6.** Comparison of the experimental and the analytical degradation of the tensile (a) strength, (b) modulus and the flexural (c) strength, (d) modulus.

More specifically, for the tension specimens, moisture diffusion was modeled using a one-dimensional Fickian formulation, assuming dominant through the thickness transport and uniform diffusion properties. The deviation from the analytical prediction is mainly associated with edge dominated moisture ingress and local divergencies in the SMC microstructure, which are not captured by the one-dimensional assumption. Due to the small thickness and higher aspect ratio of these specimens, moisture transport from exposed edges contributes to the overall uptake. Additionally, in areas that contain higher resin concentration and at fiber-matrix interfaces, diffusion may be locally accelerated, leading to higher moisture uptake at intermediate exposure times.

In the three-point bending specimens, a three-dimensional Fickian diffusion model was employed to account for the lower length to thickness aspect ratio. Despite this more comprehensive formulation, deviations from the analytical prediction are still observed. These differences are attributed to the non-uniform through the thickness moisture gradients that delay saturation in the specimen's core but reach saturation earlier at the surface layers. This delayed equilibration, combined with the heterogeneous distribution of fibers and filler particles, results in a progressive deviation from the ideal Fickian response, particularly at longer immersion times, when diffusion becomes more dependent on internal transport mechanisms.

These observations highlight the geometry-dependent nature of moisture diffusion in chopped fiber SMCs. It should be noted that one-dimensional and three-dimensional Fickian diffusion models were adopted for the tension and three-point-bending specimens, respectively, in accordance with their geometries. Therefore, the discrepancies between experimental and analytical results are attributed to edge effects and microstructural heterogeneity that is not fully captured by the diffusion formulations.

### *3.4.2. Prediction of property degradation*

Fig. 6 presents a comparison of the theoretical and experimental mechanical properties of the composite after 1000, 2000 and 3000 h of moisture absorption. The analytical models were effective at estimating both strength and modulus, particularly at saturation, which occurs after 2000 h. At this stage, the linear and exponential models show relatively low deviations from the experimental values, with the linear model performing slightly better in both tension, 0.30 % for modulus and 2.24 % for strength and three-point bending, 0.86 % for modulus and 0.91 % for strength. In tension, the exponential model deviates from the experimental value at saturation by 7.03 % for the elastic modulus and 3 % for the strength. For the flexural properties, the exponential model deviates 11.02 % and 3.31 % from the calculated modulus and strength from the test method. However, the models' predictive accuracy is less consistent during the transitional stage of 1000 h. More specifically, the tensile strength shows a 16.01 % and 21.03 % variation from the test results between the exponential and linear models, respectively and tensile modulus shows a 14.01 % and 11 % variation accordingly. In contrast, the flexural properties are well predicted even at 1000 h of conditioning with 3.52 % and 8.13 % variation in the modulus for the exponential and linear models, and 2.41 % and 7.63 % in the flexural strength. This difference in the models' predictive capability is likely due to the fact that flexural properties are often matrix-dominated, which is closely related to the degradation criteria of the polymer matrix mentioned. On the contrary, tensile properties are fiber-dominated and more sensitive to microstructural changes and less predictable failure mechanisms, especially in the early stages of degradation. Overall, the estimation is very good for both, with the exception of the tensile strength prediction in the early stages of absorption, however the linear model requires data from multiple experiments (at dry and saturation state), while the exponential model is more predictive, needing only the initial properties of the composite.

## 4. Numerical modelling

In this study, all geometries were generated and meshed in ANSYS Workbench, while the impact simulations were conducted using the LS-DYNA explicit solver, which is highly effective for non-linearities, a common characteristic in impact problems. To ensure numerical stability, a conservative Time Step Scale Factor (TSSFAC) of 0.70 was used, satisfying the Courant condition which supports that the time step must be smaller than the time required for an acoustic wave to pass through

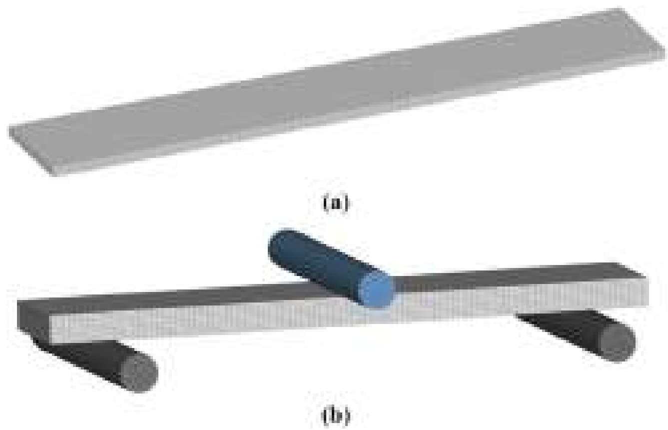


**Fig. 7.** FE models of (a) tension, (b) three-point bending.

**Table 3**
Steel input parameters for MAT_20.

| Parameter | Value |
|---|---|
| Density, RO | 7580 kg/m$^3$ |
| Young's modulus, E | 200 GPa |
| Poisson's ratio, PR | 0.33 (−) |

**Table 4**
MAT_162 input parameter for different conditioning times.

| Parameter | Value | | | |
|---|---|---|---|---|
| | 0 h | 1000 h | 2000 h | 3000 h |
| Density, RO | 1878 kg/m$^3$ | 1878 kg/m$^3$ | 1878 kg/m$^3$ | 1878 kg/m$^3$ |
| Young's modulus - longitudinal direction, $E_a$ | 12.2 GPa | 9.2 GPa | 8 GPa | 8 GPa |
| Young's modulus - transverse direction, $E_b$ | 12.2 GPa | 9.2 GPa | 8 GPa | 8 GPa |
| Young's modulus - through thickness direction, $E_c$ | 5 GPa | 3.4 GPa | 3.4 GPa | 3.4 GPa |
| Poisson's ratio, $v_{ba}$ | 0.15 (−) | 0.15 (−) | 0.15 (−) | 0.15 (−) |
| Poisson's ratio, $v_{ca}$, $v_{cb}$ | 0.18 (−) | 0.18 (−) | 0.18 (−) | 0.18 (−) |
| Shear modulus, $G_{ab}$ | 5.8 GPa | 4 GPa | 4 GPa | 4 GPa |
| Shear modulus, $G_{bc}$, $G_{ca}$ | 3.5 GPa | 2.4 GPa | 2.4 GPa | 2.4 GPa |
| Longitudinal tensile strength, $S_{aT}$ | 95 MPa | 58 MPa | 46 MPa | 45 MPa |
| Transverse tensile strength, $S_{bT}$ | 95 MPa | 58 MPa | 46 MPa | 45 MPa |
| Through thickness tensile strength, $S_{cT}$ | 75 MPa | 51 MPa | 51 MPa | 51 MPa |
| Longitudinal compressive strength, $S_{aC}$ | 133 MPa | 89 MPa | 89 MPa | 89 MPa |
| Transverse compressive strength, $S_{bC}$ | 133 MPa | 89 MPa | 89 MPa | 89 MPa |
| Matrix mode shear strength, $S_{ab}$, $S_{bc}$, $S_{ca}$ | 75 MPa | 51 MPa | 51 MPa | 51 MPa |

the smallest element. For the structural discretization, solid elements with ELFORM = 1, a reduced integration formulation with a single integration point, were employed. Although computationally efficient, hourglass modes can arise from this formulation, which requires stabilization. To prevent this, a stiffness-based hourglass control (Type 4) was adopted, which is particularly effective in impact simulations involving structural components. A reduced hourglass coefficient of 0.05 was used to limit artificial stiffness while preserving the physical fidelity of the simulation.

A previously validated model, developed from drop tower impact tests reported in an earlier work [54], is employed for the analysis. In the model, a comparison between the housing response under varying impact energy levels and the corresponding experimental data showed strong agreement, confirming the reliability of the FE models developed.

### 4.1. Tension and three-point bending models with degraded properties

In order to reproduce the static tensile and flexural tests, two models were developed, with their configuration presented in Fig. 7. For the simulation of the tensile loading, only the gage length of the specimen is modeled, to avoid modelling the grips as well. More specifically, a specimen measuring 150 mm × 25 mm × 2.5 mm, was meshed with 1 mm solid elements and had its cross section on one side constrained (BOUNDARY_SPC_SET). The other side's cross section nodes were assigned to move in the x-direction (BOUNDARY_PRESCRIBED_MOTION_SET). In order to obtain the force-displacement curve the resulting force from the nodes on the moving side were plotted with displacement. The three-point bending configuration consisted of two cylindrical supports of a 6 mm diameter and a cylindrical punch with the same diameter, that replicates the dimensions of the experimental setup. The three components were modeled as rigid bodies (MAT_20_RIGID), with properties stated in Table 3, and discretized with 1 mm elements. The two supports were fully constrained, while the punch was only allowed to move in the z-direction. An automatic contact was assigned between the specimen and the rigid bodies (CONTACT_AUTOMATIC_SURFACE_TO_SURFACE).

Both SMC composite specimens, in the tension and three-point bending cases, were modeled using MAT_162 (MAT_COMPOSITE_MSC_DMG), which allows progressive failure analysis of composite materials. This formulation incorporates Hashin failure criteria together with a damage mechanics–based softening law that controls the material response after damage initiation. Due to the randomly oriented chopped glass fibers in the SMC, the material exhibits transversely isotropic behavior, characterized by identical in-plane properties but reduced out-of-plane strength, resembling a unidirectional-like response. This was represented in the model through AMODEL option 1, which implies transverse isotropy.

The properties for the dry state were determined by standardized tests in tensile, flexural, compressive and shear loading, presented in Ref. [54]. The degraded tensile and flexural properties after 1000, 2000 and 3000 h of moisture absorption, were determined in Section 2.3, while the remaining properties required by the model, were calculated using the exponential degradation model and Eq. (17), based on the initial properties obtained from testing, listed in Table 4. This approach was selected because it requires limited experimental input, relying only on the reference (dry) material state, while still enabling effective extrapolation of degradation with increasing moisture content. However, it should be noted that this approach assumes uniform degradation across all properties, irrespective of loading mode. More specifically, a degradation parameter of k = 0.9 was assumed for all strengths and k = 0.6 for all moduli, to account for differing sensitivity to moisture exposure, based on the fitting of the k parameter addressed in Section 3.4.2. Although this simplification does not capture property degradation in detail, it provides a practical and computationally efficient framework for integrating moisture effects into structural-level simulations. To evaluate the validity of this assumption, tensile and three-point bending models were developed, enabling the comparison between the calculated inputs at prolonged conditioning times and the corresponding experimental results.

Figs. 8 and 9 present comparisons between experimental and FE results for tensile and three-point bending specimens at different stages of moisture conditioning. Across all conditioning times, the numerical predictions closely reproduce the experimental force–displacement curves, confirming the reliability of the material modeling approach and the accuracy of the degradation parameters derived from testing.

For tensile loading, in Fig. 8, the numerical curves capture both the degradation and the overall shape of the experimental curves with the increase of moisture absorption, with good accuracy. The peak loads decrease with conditioning time, reflecting the loss of tensile strength

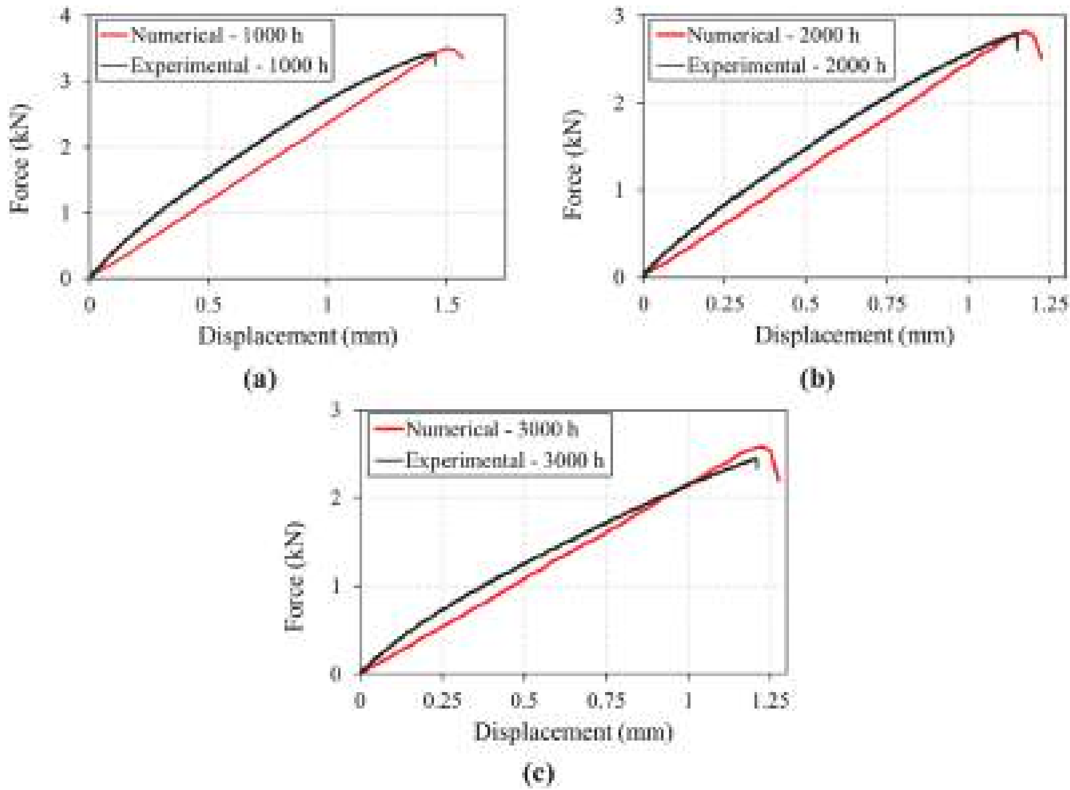


**Fig. 8.** Comparison of the experimental and numerical force-displacement curves derived from tensile loading with degraded properties after (a) 1000h, (b) 2000h, (c) 3000h of conditioning.

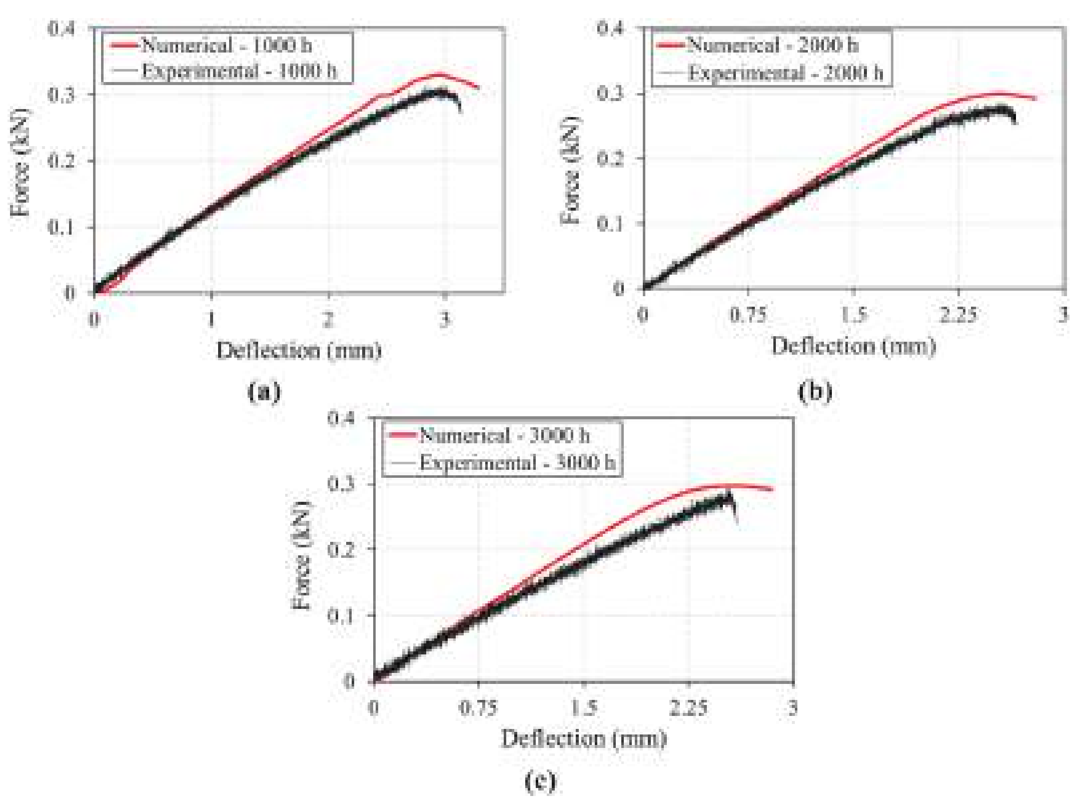


**Fig. 9.** Comparison of the experimental and numerical force-displacement curves derived from three-point bending with degraded properties after (a) 1000h, (b) 2000h, (c) 3000h of conditioning.

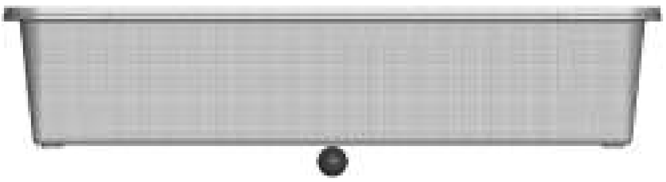

**Fig. 10.** FE mesh of the housing and the impactor of the ground impact model.

**Table 5**
Delamination damage model input data for Tiebreak contact.

| Parameter | Value |
|---|---|
| Normal failure stress (peak traction), NFLS | 40 MPa |
| Shear failure stress (peak traction), SFLS | 60 MPa |
| Exponent of the mixed mode criterion (Power law), PARAM | 2 |
| Normal energy release rate, ERATEN | 1.7 MPa mm |
| Shear energy release rate, ERATES | 0.789 MPa mm |
| Tangential stiffness to normal stiffness, CT2CN | 1 |
| Normal stiffness, CN | $10^6$ MPa/mm |

with a percentage of variation concerning the FE models and the experiments between 2.10 and 6.51 %. However, even though numerical and experimental stiffness are well aligned, small deviations suggest that localized damage, such as fiber–matrix debonding and microcrack propagation, as well as the elastoplastic behaviour of the SMC composite are not fully captured by the homogenized material model, MAT_162. Nevertheless, the close agreement confirms the capability of the degradation law for predicting strength evolution under tensile loading.

Regarding the comparison between experimental and numerical flexural responses under three-point bending, in Fig. 9, the agreement is even stronger. The numerical curves closely match both the peak load and post-peak behavior, with a deviation between 1.02 and 4.14 %. Overall, the ability of the numerical model to reproduce both matrix- and fiber-dominated degradation is a strong indication of its predictive capability for more complex structural simulations.

### 4.2. Impact response with degraded properties

#### 4.2.1. Ground impact

Ground impact simulations are critical for evaluating the crashworthiness of electric vehicle battery housings, given the vulnerability of lithium-ion cells to hazardous failure modes. Under real-world conditions, impacts from road debris can inflict severe damage on the housing, potentially propagating damage to the cells and triggering short circuits, electrolyte leakage, or thermal runaway. Even sub-critical impacts can still degrade performance and reduce service life. Therefore, finite element simulations provide an important tool to predict structural response, optimize the housing configuration, and mitigate both progressive and catastrophic failure.

In this study, the ground impact FE model comprises three primary components, as shown in Fig. 10, the composite housing, an adhesively bonded lid, and a spherical steel impactor with a 20 mm diameter that weighs 0.3 kg. The steel impactor, that serves as road debris in this impact scenario, is defined as a rigid body (MAT_RIGID) constrained in the z-direction to achieve only vertical motion and is meshed with 1 mm solid elements, with the properties used described in Table 3. The housing and lid assembly is modeled using MAT_162, with the properties stated in Tables 4 and is discretized with 2 mm solid elements in a hexagonal mapped mesh. The four bottom legs of the battery housing

**Table 6**
Material input data for ABS properties.

| Parameter | Value |
|---|---|
| | MAT_12 |
| Density, RO | 1040 kg/m$^3$ |
| Shear modulus, G | 0.85 GPa |
| Yield stress, SIGY | 41.5 MPa |
| Bulk modulus, BULK | 3.94 GPa |
| | MAT_ADD_EROSION |
| Equivalent stress at failure, SIGVM | 55 MPa |

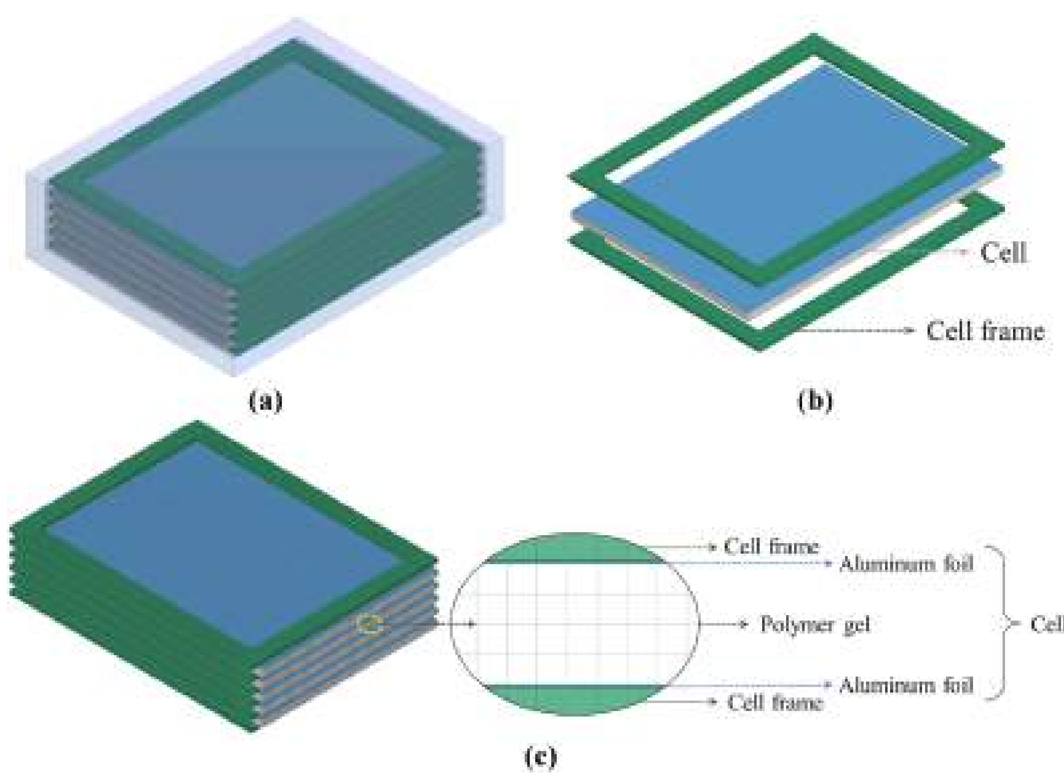


**Fig. 11.** Geometry of (a) the cell pack, (b) the cell frames, and (c) the cells.

**Table 7**
Material parameters of the cell components implemented in MAT_01.

| Parameter | Value | |
|---|---|---|
| | Aluminum foil | Polymer gel |
| Density, RO | 2700 kg/m$^3$ | 900 kg/m$^3$ |
| Young's modulus, E | 69 GPa | 1.5 GPa |
| Poisson's ratio, PR | 0.33 (−) | 0.45 (−) |

were fully constrained in the z-direction to simulate fixed support conditions using the BOUNDARY_SPC_SET command. Due to the dynamic loading, CERATE parameters, of values between 0.024 and 0.03, were implemented in MAT_162 to add the ability of predicting the effects of the strain-rate dependent non-linear stress-strain response of the composite, which is modeled by a logarithmic strain-rate dependent function for the moduli and strength. Furthermore, the interaction between the impactor and the housing is captured using CONTACT_AUTOMATIC_SURFACE_TO_SURFACE, while adhesive bonding is achieved by CONTACT_AUTOMATIC_SURFACE_TO_SURFACE_TIEBREAK (Option 9) with properties stated in Table 5, employing a bilinear traction–separation law and progressive damage formulation to simulate interfacial failure mechanisms. This approach provides computational efficiency while preserving the accuracy of cohesive zone modeling for debonding behavior.

The internal assembly consists of a thermoplastic ABS cell pack containing five pouch cells with aluminum–plastic enclosures and Li/Advanced LFP chemistry, as shown in Fig. 11. For modeling purposes, each cell is simplified as a 0.1 mm aluminum film with an 8 mm polymer gel core, constrained by ABS plastic frames positioned between the cells. The cell pack and the cell frames are meshed with 3 mm elements and 2 mm elements for the pouch cells, while the ABS material is modeled

**Table 8**
Permanent deformation in the z-direction after 15 and 25 m/s ground impact for different conditioning times.

| Impact velocity | | Permanent deformation | | | |
|---|---|---|---|---|---|
| | | 0 h | 1000 h | 2000 h | 3000 h |
| i. | 15 m/s | 0.57 mm | 0.32 mm | 0.29 mm | 0.25 mm |
| ii. | 25 m/s | 1.07 mm | 1.66 mm | 1.97 mm | 2.03 mm |

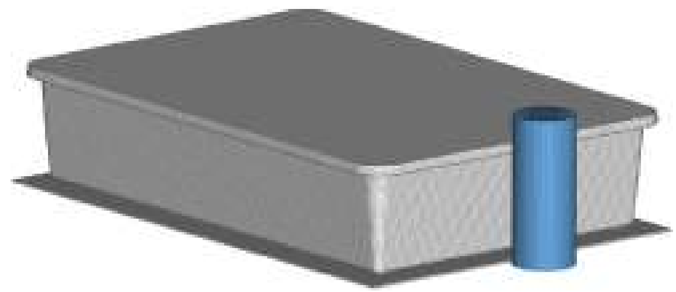

**Fig. 13.** FE mesh of the housing and the impactor of the pole impact model.

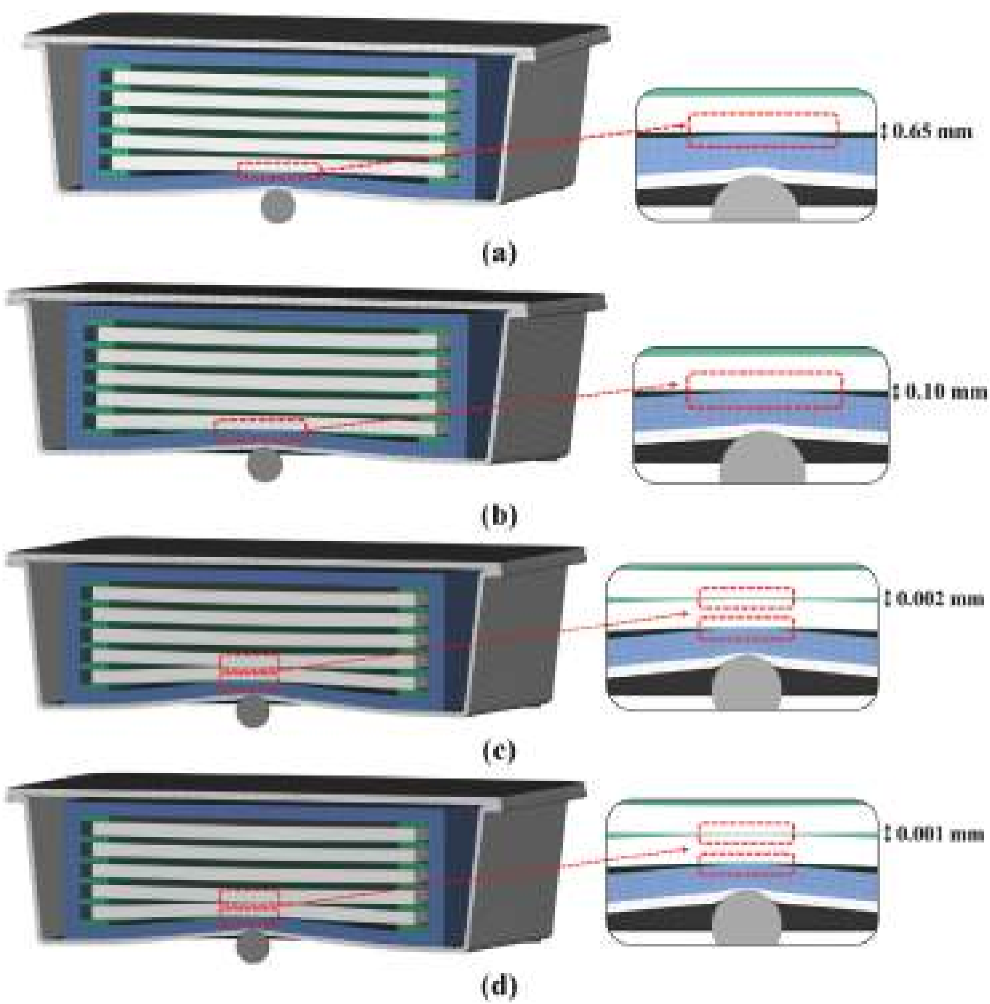


**Fig. 12.** Response of the 15 m/s ground impact at (a) 0 h, (b) 3000 h and the 25 m/s ground impact at (c) 0 h and (d) 3000 h of water conditioning.

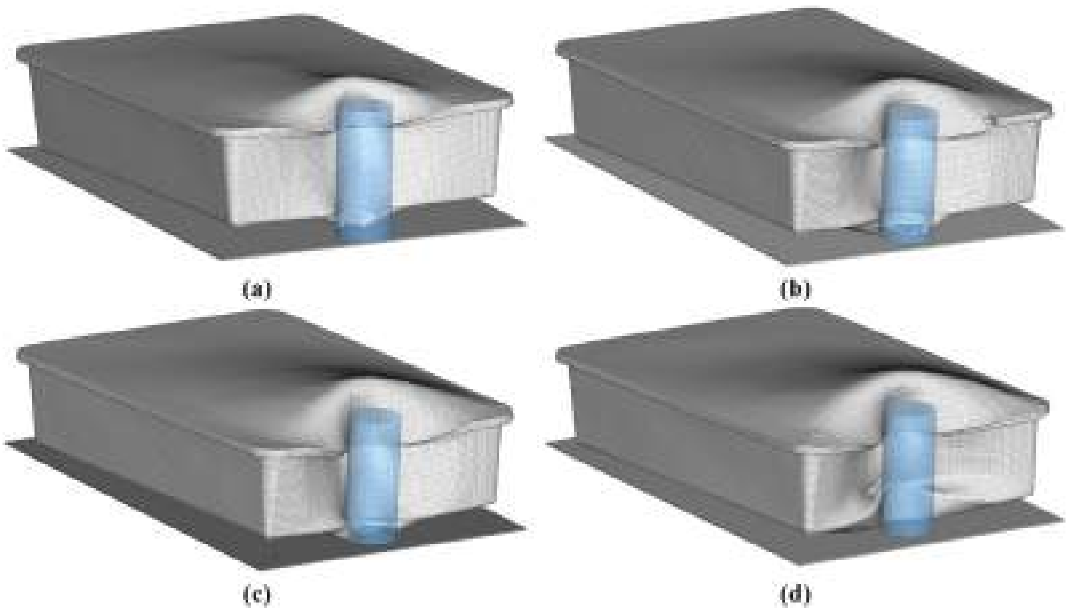

Fig. 14. Maximum deformation of the housing in the 10 m/s pole impact for (a) 0 h, (b) 1000 h, (c) 2000 h and (d) 3000 h of water conditioning.

using an isotropic elastic-plastic material, MAT_24, with ADD_EROSION activated to capture element deletion based on the von Mises stress criterion, as described in Table 6. The film and gel components are defined using MAT_01 and properties shown in Table 7, an elastic material model, with CONTACT_TIED_SURFACE_TO_SURFACE applied to ensure kinematic compatibility between the two components. Additional automatic contact definition allows relative motion and load transfer between the cells, frames, and housing, while the tiebreak formulation represents adhesive bonding on the inside of the housing and the cell pack interface. Overall, this modeling approach, although simplified, enables realistic simulation of impact-induced failure mechanisms in the battery system.

A parametric study is conducted to evaluate the ground impact response of two impact energy levels, corresponding to intermediate and high impactor velocities of 15 and 25 m/s. For each case, four material conditions are considered, namely the dry state, after 1000 h of water conditioning, and after extended exposure of 2000 and 3000 h. The results were then compared to evaluate the influence of moisture degradation on damage behavior.

*4.2.1.1. Ground impact results.* Fig. 12 illustrates the maximum deformation of the housing under ground impact at 15 and 25 m/s in both dry (0 h) and saturated (3000 h) states. At 15 m/s, the housing at dry state shows a maximum displacement of 6.86 mm, while the cell pack shows a displacement of 5.74 mm, which results in a 0.65 mm residual gap between the cell pack and the first cell in the stack (Fig. 12(a)). At saturation, in Fig. 12(b), the housing and the cell pack are displaced 7.76 mm and 5.92 mm, respectively, resulting in a 0.10 mm gap between the cell pack and the first pouch cell. Although the integrity of the cells is preserved, there is a significant difference in the extent of deformation due to the degraded mechanical properties of the SMC. At 25 m/s, the housing's maximum displacement, at dry state, increases to 11.20 mm, while the cell pack reaches 8.20 mm. The first cell is significantly deformed, and the load propagates to the second cell, leaving a 0.002 mm gap between the two cells (Fig. 12(c)). Similarly, in saturation state, the housing is deformed up to 11.71 mm and the cell pack at 8.56 mm, which leads to a 0.001 mm gap between the first and the second cell in the stack (Fig. 12(d)).

Table 8 reports the permanent deformation of the housing after 15 m/s and 25 m/s ground impacts. At the 15 m/s impact, the decrease in permanent deformation of the housing with increasing moisture absorption, from 0.57 mm at dry state to 0.25 mm at saturation state, can be explained by the transition from ductile to brittle failure behavior induced by water ingress. According to Table 4, the tensile modulus decreases from 12.2 GPa to 8.0 GPa after 3000 h of conditioning, while the tensile strength drops from 95 MPa to 45 MPa. These reductions correspond to a stiffness loss of approximately 35 % and a strength loss of more than 50 %. This behaviour shows the embrittlement of the resin matrix and the reduced ductility of the fiber–matrix interface due to moisture-induced microcracking and interfacial debonding, at a macroscopic level. The von Mises stress also supports this interpretation, falling from 120 MPa, at 0 h, to 100 MPa, at 3000 h, indicating that the conditioned material fails earlier through local damage rather than sustaining high stresses through plastic deformation. Thus, in a moderate impact, energy absorption becomes dominated by fracture and damage initiation instead of plastic deformation, leading to smaller residual indentation despite the overall reduction in strength.

In contrast, at the higher impact velocity of 25 m/s, the same material degradation leads to a notable increase in permanent deformation, from 1.07 mm in the dry state to 2.03 mm at 3000 h of moisture conditioning. Under higher energy conditions, the reduced loadbearing capability of the structure is exceeded. The reduced modulus and strength promote matrix cracking and progressive structural deterioration, which is reinforced by the Von Mises stresses that decrease from 160 MPa in the dry state to 120 MPa at saturation, indicating that the housing is not able to maintain high stresses but undergoes large global deformations. This change in behavior underlines the transition from localized, brittle failure at moderate energy to extensive damage due to plastic deformation at higher energy levels. This results in contrasting deformations and a different macroscopic outcome, where embrittlement dominates moderate energy responses and loss of structural integrity governs high energy impacts.

Overall, the influence of the material degradation induced by moisture uptake is primarily reflected in the global bending response of the battery housing. The reduction in elastic modulus and strength of the SMC material decreases the structural stiffness, allowing larger flexural deformation when the housings comes in contact with the impactor. Therefore, increased vertical displacement is transmitted to the cell pack. This response indicates that degradation due to moisture absorption at the material level translates into a reduced ability of the structure to distribute and absorb impact energy, affecting the crashworthiness performance of the battery housing.

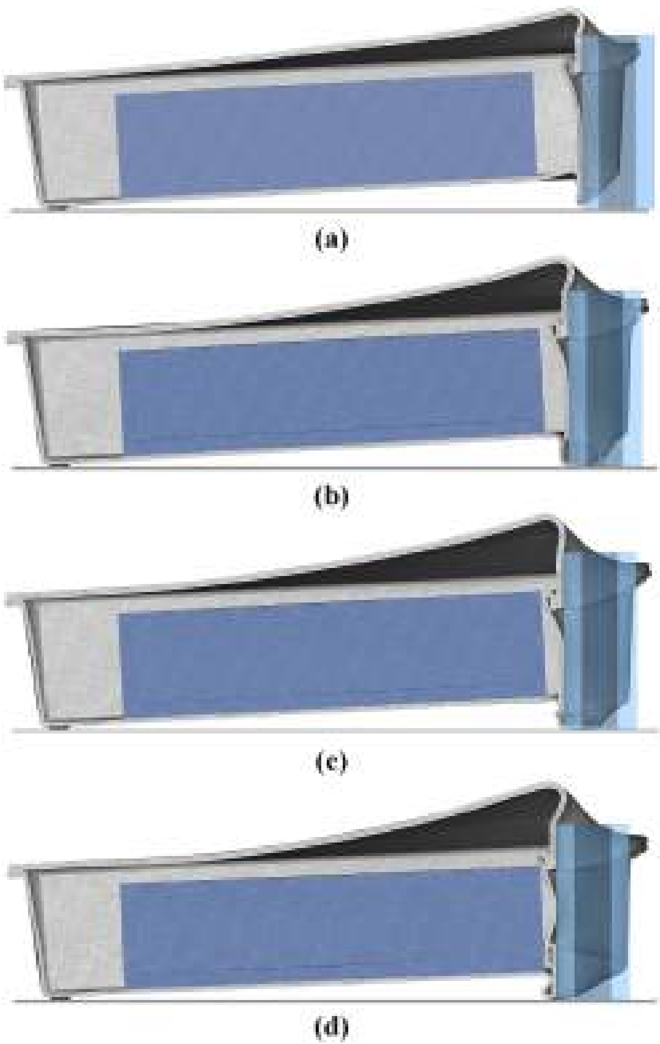


**Fig. 15.** Maximum displacement of the housing and the cell pack in the event of 10 m/s pole impact for (a) 0 h, (b) 1000 h, (c) 2000 h, (d) 3000 h of water conditioning.

*4.2.2. Pole impact*

Pole impact simulations are among the most challenging crash scenarios for battery enclosures, as they involve localized, high-energy loadings that are representative of real-world collisions. These simulations are crucial for evaluating the enclosure's crashworthiness in terms of energy absorption, structural integrity, and cell pack protection, while also accounting for material efficiency. In this study, a parametric analysis is performed on the SMC composite housing under two impact velocities, 10 and 15 m/s, replicating conditions observed in full-scale vehicle crash tests to evaluate structural resilience at different moisture absorption states, from 0 to 3000 h of conditioning.

The FE model includes the SMC housing and the adhesively bonded lid, a cylindrical impactor, and a rigid base plate representing the vehicle floor, as shown in Fig. 13. The steel impactor is modeled as a rigid body with steel properties and is 120 mm in length, has a 50 mm diameter and weighs 7 kg. It is allowed to move in the x-direction, using an initial velocity (INITIAL_VELOCITY_GENERATION), while the rigid, steel base plate, measuring 440 × 300 mm, is fully constrained in all translational degrees of freedom. Concerning discretization, all parts are meshed with 2 mm solid elements. Contact between the impactor and the housing assembly is defined using CONTACT_AUTOMATIC_SURFACE_TO_SURFACE, with adhesive joints, between the housing and the lid, as well as the cell pack and the housing modeled via a tiebreak contact to allow debonding under high loads. The housing is additionally bonded to the base plate using adhesive film properties, stated in Table 5, to ensure realistic interface behavior during impact.

*4.2.2.1. Pole impact results.* Fig. 14 shows the evolution of the maximum deformation of the housing under a 10 m/s pole impact across different conditioning times. The impactor displacement is increased progressively from 47.20 mm at 0 h to 69.30 mm after 3000 h, reflecting the reduction of stiffness due to moisture absorption. This aligns with the material degradation shown in Table 4, where the longitudinal modulus decreases from 12.2 GPa at 0 h to 8 GPa after 3000 h, and the tensile strength is reduced by nearly 50 %, which explains the higher penetration observed. Despite that, the housing's structural integrity is predominantly preserved, even after 3000 h. This suggests that the SMC housing retains its protective capability and its ability to dissipate energy, indicating that the design safety margins are sufficient for low to intermediate crash severities, despite the reduction of the system's robustness due to long-term moisture absorption.

The intersection of the housing and the cell pack shown in Fig. 15 provides additional information by tracking the response of the cells and their interaction with the housing. It is evident that prolonged moisture exposure gradually compromises the load transfer efficiency between the housing and the pack. In the z-direction, cell displacements decrease from 10.10 mm at 0 h to 8.30 mm at 3000 h, while lateral displacements in the x-direction reduce from 2.36 mm to 1.84 mm. These values indicate that the pack remains effectively shielded. The slight reduction in cell motion, despite greater impactor penetration, suggests that with the increase of moisture absorption stress distribution is altered and local failure modes are amplified within the structure. The difference between the dry and the moisture-aged housing is also apparent in the distance that is left between the housing walls and the cell pack at the maximum displacement of the impactor. While in Fig. 15(a) the distance provides reassurance that the cell pack remains intact, the distance in Fig. 15(d) is almost eliminated, making the 10 m/s impact the new threshold that ensures cell safety.

On the contrary, the 15 m/s case shown in Fig. 16 reveals the damaging effects of moisture uptake. The impactor displacement increases from 79.1 mm at 0 h to 94.4 mm at 3000 h, demonstrating a noticeable loss of stiffness and energy absorption. The degradation is consistent with the FE material inputs, where tensile and compressive strengths drop by almost half over the conditioning period, substantially lowering the resistance to concentrated loading. At this higher velocity, the housing's response evolves from a localized deformation of the housing's walls to a broader and less predictable deformation field, which clearly indicates compromised structural integrity.

Fig. 17 presents the deformation of the cell pack. Unlike the 10 m/s case, here the displacement of the cell pack grows significantly with aging time, indicating that the degraded housing is unable to protect the internal assembly effectively. At 0 h the cells move 9.7 mm in z-direction, showing a small indentation of 3 mm in the lower half of the pack, due to interaction with the impactor, as depicted in Fig. 17(a). With conditioning, however, the cell pack gets deformed significantly with the z-displacement peaking at 11.5 mm at 2000 h, and the x-displacement reaching 8.9 mm after 3000 h of conditioning. These elevated lateral deformations are concerning as they suggest instability in the cell pack, raising the risk of mechanical damage, internal short circuits, or thermal runaway. Together, Figs. 16 and 17 confirm that at 15 m/s the moisture-driven degradation transforms an impact that could not induce catastrophic damage to the cell pack, into potential failure, underlining the importance of accounting for long-term environmental effects in the crashworthiness assessment of composite battery housings.

To conclude, the pole impact scenario is characterized by high loading, where moisture-induced degradation affects stiffness and load distribution capacity in the impact area, altering the balance between elastic energy storage, damage initiation, and plastic deformation. The

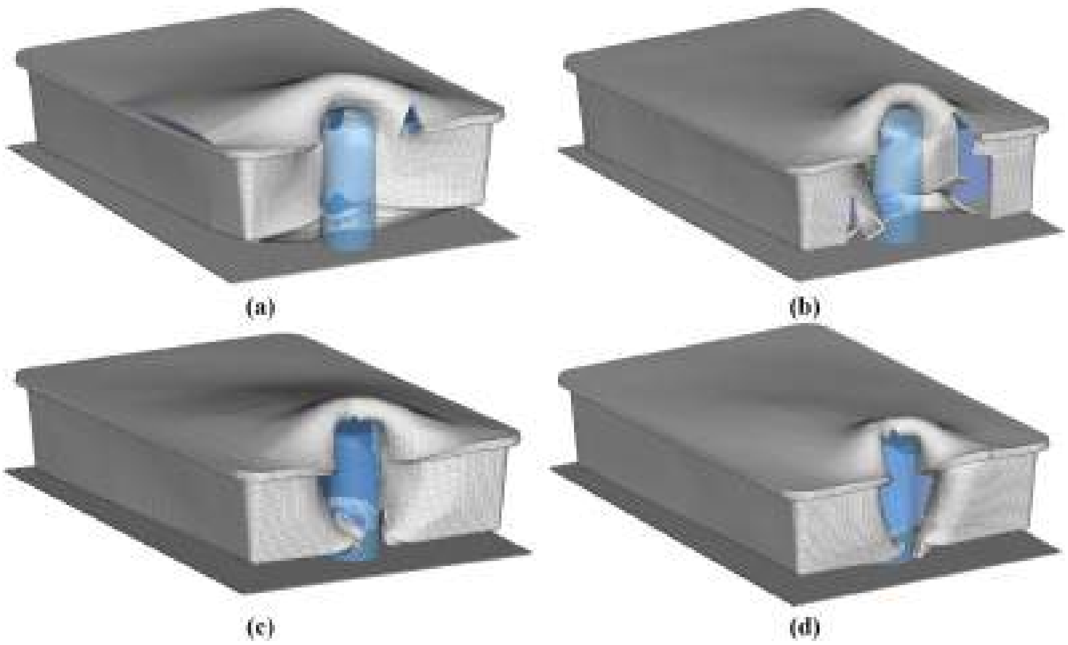


**Fig. 16.** Maximum deformation of the housing in the 15 m/s pole impact for (a) 0 h, (b) 1000 h, (c) 2000 h and (d) 3000 h of water conditioning.

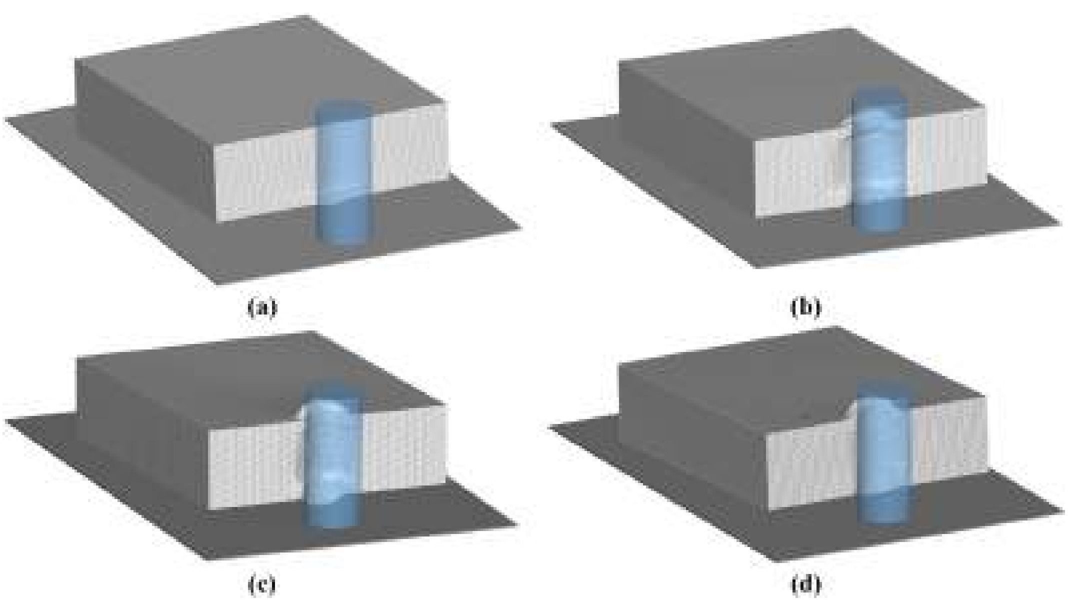


**Fig. 17.** Maximum deformation of the cell pack in the 15 m/s pole impact for (a) 0 h, (b) 1000 h, (c) 2000 h and (d) 3000 h of water conditioning.

reduced material stiffness leads to increased local deformation and stress concentration around the contact zone of the pole, limiting the ability of the surrounding structure to effectively distribute the impact load, leading to earlier damage initiation. As a result, the degraded material exhibits a more prominent damage, which influences the overall crash behaviour of the battery housing and alters the deformation pattern compared to the dry case, affecting the cell pack's structural integrity as well.

## 5. Conclusions

This study investigates the moisture absorption behavior of sheet molding compound (SMC) thermoplastic composites and its influence on the crash performance of an electric vehicle battery housing, demonstrating high sensitivity to prolonged moisture exposure both on material behaviour and structural performance. Water immersion up to 3000 h led to an initial Fickian diffusion stage followed by deviations associated with matrix plasticization and microstructural damage. At saturation, tensile and flexural strengths were reduced by approximately 50 %, while the elastic moduli exhibited degradation of about 35 %. Although desorption resulted in partial recovery of stiffness and strength, the permanent mass loss and low mechanical properties indicate that moisture-induced damage mechanisms are not fully reversible.

The experimental results were successfully reproduced by analytical diffusion and degradation models, providing predictive capability of the moisture uptake and mechanical property evolution over time. Among the degradation models considered, the linear formulation showed good agreement at saturation, while the exponential model offered predictions with fewer input parameters. When these degraded properties, that derived from both testing and the exponential model, were implemented in finite element models, the simulations replicated the experimentally observed mechanical response and revealed a significant reduction in crashworthiness with increasing exposure time.

At the structural level, impact simulations showed that moisture aging significantly alters the crash response of the battery housing. While low-energy impacts showed that the cell pack remains intact even after prolonged conditioning, higher-velocity ground and pole impacts resulted in increased housing deformation and reduced protection of the internal cell pack. These findings indicate that environmental aging can critically undermine the safety margins of SMC battery enclosures, that leads to the need for moisture-induced degradation incorporation into durability-driven design, material selection and safety assessment, which is essential for ensuring long-term safety, reliability, and overall performance of electric vehicle structures.

## CRediT authorship contribution statement

**Aikaterini Fragiadaki:** Writing – original draft, Software, Methodology, Investigation. **Konstantinos Tserpes:** Writing – review & editing, Validation, Supervision, Methodology, Investigation, Funding acquisition.

## Funding

This work was financially supported by the EC-funded HORIZON Project “TEMPEST” -Project 101103681-. [HORIZON-CL5-2022-D2-01-05 — Next generation technologies for High-performance and safe-by-design battery systems for transport and mobile applications (Batteries Partnership)].

## Declaration of competing interest

The authors declare the following financial interests/personal relationships which may be considered as potential competing interests: Konstantinos Tserpes reports financial support was provided by University of Patras. If there are other authors, they declare that they have no known competing financial interests or personal relationships that could have appeared to influence the work reported in this paper.

## Acknowledgments

All authors acknowledge support from Fraunhofer ICT, who provided the material samples and the CAD file of the housing to perform the mechanical tests and simulations.

## Data availability

Data will be made available on request.

## References

[1] Duncan BC, Broughton WR. Absorption and diffusion of moisture in polymeric materials. Teddington, UK: National Physical Laboratory; 2023. https://doi.org/10.47120/npl.mgpg102.
[2] Korkees F. Moisture absorption behavior and diffusion characteristics of continuous carbon fiber reinforced epoxy composites: a review. Polym Plastics Technol Mater 2023;62:1789–822. https://doi.org/10.1080/25740881.2023.2234461.
[3] Pérez-Pacheco E, Cauich-Cupul JI, Valadez-González A, Herrera-Franco PJ. Effect of moisture absorption on the mechanical behavior of carbon fiber/epoxy matrix composites. J Mater Sci 2013;48:1873–82. https://doi.org/10.1007/s10853-012-6947-4.
[4] Zhang S, Liu Y, Feng P, Prabhakar P. Moisture diffusion in multi-layered materials: the role of layer stacking and composition. Compos B Eng 2025;293:112128. https://doi.org/10.1016/j.compositesb.2025.112128.
[5] Post NL, Riebel F, Zhou A, Keller T, Case SW, Lesko JJ. Investigation of 3D moisture diffusion coefficients and damage in a pultruded E-glass/Polyester structural composite. J Compos Mater 2009;43:75–96. https://doi.org/10.1177/0021998308098152.
[6] Bel Haj Frej H, Léger R, Perrin D, Ienny P. A novel thermoplastic composite for marine applications: comparison of the effects of aging on mechanical properties and diffusion mechanisms. Appl Compos Mater 2021;28:899–922. https://doi.org/10.1007/s10443-021-09903-0.
[7] Janas VF. Moisture absorption in unfilled and glass-filled, cross-linked polyester n.d.
[8] Chaichanawong J, Thongchuea C, Areerat S. Effect of moisture on the mechanical properties of glass fiber reinforced polyamide composites. Adv Powder Technol 2016;27:898–902. https://doi.org/10.1016/j.apt.2016.02.006.
[9] Shen C-H, Springer GS. Moisture absorption and desorption of composite materials n.d.
[10] Chilali A, Assarar M, Zouari W, Kebir H, Ayad R. Effect of geometric dimensions and fibre orientation on 3D moisture diffusion in flax fibre reinforced thermoplastic and thermosetting composites. Compos Appl Sci Manuf 2017;95:75–86. https://doi.org/10.1016/j.compositesa.2016.12.020.
[11] Abdessalem A, Tamboura S, Shirinbayan M, Laribi MA, Ben Daly H, Fitoussi J. Coupled effects of hygrothermal degradation and fatigue damage of sheet molding compound (SMC) composite. Eur J Mech Solid 2025;109:105480. https://doi.org/10.1016/j.euromechsol.2024.105480.
[12] Fragiadaki A, Tserpes K. Impact response of a thermoplastic battery housing for transport applications. Batteries 2025;11:369. https://doi.org/10.3390/batteries11100369.
[13] Alawsi G, Aldajah S, Rahmaan SA. Impact of humidity on the durability of E-glass/polymer composites. Mater Des 2009;30:2506–12. https://doi.org/10.1016/j.matdes.2008.10.002.
[14] Mohammadkhani P, Magliaro J, Rahimidehgolan F, Khapra T, Altenhof W. Moisture influence on anisotropic mechanical behavior of direct compounded compression molded PA6/Glass LFTs. Compos B Eng 2023;264:110927. https://doi.org/10.1016/j.compositesb.2023.110927.
[15] Kazemi ME, Shanmugam L, Lu D, Wang X, Wang B, Yang J. Mechanical properties and failure modes of hybrid fiber reinforced polymer composites with a novel liquid thermoplastic resin. Elium® Composites Part A: Appl Sci Manuf 2019;125:105523. https://doi.org/10.1016/j.compositesa.2019.105523.
[16] Nash NH, Portela A, Bachour-Sirerol CI, Manolakis I, Comer AJ. Effect of environmental conditioning on the properties of thermosetting- and thermoplastic-matrix composite materials by resin infusion for marine applications. Compos B Eng 2019;177:107271. https://doi.org/10.1016/j.compositesb.2019.107271.
[17] Davies P, Le Gac P-Y, Le Gall M. Influence of sea water aging on the mechanical behaviour of acrylic matrix composites. Appl Compos Mater 2017;24:97–111. https://doi.org/10.1007/s10443-016-9516-1.
[18] Davies P, Arhant M. Fatigue behaviour of acrylic matrix composites: influence of seawater. Appl Compos Mater 2019;26:507–18. https://doi.org/10.1007/s10443-018-9713-1.
[19] Chilali A, Zouari W, Assarar M, Kebir H, Ayad R. Analysis of the mechanical behaviour of flax and glass fabrics-reinforced thermoplastic and thermoset resins. J Reinforc Plast Compos 2016;35:1217–32. https://doi.org/10.1177/0731684416645203.
[20] Chebil MS, Bouaoulo G, Gerard P, Euch SE, Issard H, Richaud E. Oxidation and unzipping in ELIUM resin: kinetic model for mass loss. Polym Degrad Stabil 2021;186:109523. https://doi.org/10.1016/j.polymdegradstab.2021.109523.
[21] Kazemi ME, Shanmugam L, Chen S, Yang L, Yang J. Novel thermoplastic fiber metal laminates manufactured with an innovative acrylic resin at room temperature. Compos Appl Sci Manuf 2020;138:106043. https://doi.org/10.1016/j.compositesa.2020.106043.
[22] Guo K, Deng Y, Ren Y, Jiang H. Multi-scale moisture diffusion modeling and analysis of carbon/Kevlar-fiber hybrid composite laminates under the hygrothermal aging environment. Polym Degrad Stabil 2024;229:110952. https://doi.org/10.1016/j.polymdegradstab.2024.110952.
[23] Shirinbayan M, Beigi Rizi H, Abbasnezhad N, Tcharkhtchi A, Fitoussi J. Tension, compression, and shear behavior of advanced sheet molding compound (A-SMC): Multi-scale damage analysis and strain rate effect. Compos B Eng 2021;225:109287. https://doi.org/10.1016/j.compositesb.2021.109287.
[24] Penavayre C, Fitoussi J, Richaud E, Papin P, Bouneb J, Hochstetter G, et al. Long-Term behavior of carbon fiber-reinforced thermoplastic composites for type V hydrogen storage tanks: effects of hygrothermal aging on physicochemical and mechanical properties. Polym Compos 2025. https://doi.org/10.1002/pc.70229. pc.70229.
[25] Penavayre C, Fitoussi J, Richaud E, Papin P, Bouneb J, Hochstetter G, et al. Interfacial damage evolution in hygrothermally aged CF/PPA composites used in type V hydrogen tanks: a multi-scale approach. Composites Part C: Open Access 2025;18:100679. https://doi.org/10.1016/j.jcomc.2025.100679.
[26] Goh YG, Sufian AS, Mohamad N, Afiqah N. Mechanical properties of recycled polypropylene filled with aluminium hydroxide. Mater Sci Forum 2020;1010:130–5. https://doi.org/10.4028/www.scientific.net/MSF.1010.130.
[27] Guo A, Tao X, Kong H, Zhou X, Wang H, Li J, et al. Effects of aluminum hydroxide on mechanical, water resistance, and thermal properties of starch-based fiber-reinforced composites with foam structures. J Mater Res Technol 2023;23:1570–83. https://doi.org/10.1016/j.jmrt.2023.01.132.
[28] Lydersen E. The solubility and hydrolysis of aqueous aluminium hydroxides in dilute fresh waters at different temperatures. Hydrol Res 1990;21:195–204. https://doi.org/10.2166/nh.1990.0015.
[29] Chebil MS, Gerard P, Issard H, Richaud E. Thermal stability of polymethacrylic based ELIUM® resin: effect of comonomers, antioxidants and aluminum trihydrate filler. Polym Degrad Stabil 2023;213:110367. https://doi.org/10.1016/j.polymdegradstab.2023.110367.

[30] Bergeret A, Pires I, Foulc MP, Abadie B, Ferry L, Crespy A. The hygrothermal behaviour of glass-fibre-reinforced thermoplastic composites: a prediction of the composite lifetime. Polym Test 2001;20:753–63. https://doi.org/10.1016/s0142-9418(01)00030-7.

[31] Pantelakis S, Katsiropoulos CV, Tserpes KI, Felgeyrolles T. Effect of water absorption on strength of the aeronautical composite material fiberdux HTA/6376. KEM 2009;417–418:457–60. https://doi.org/10.4028/www.scientific.net/KEM.417-418.457.

[32] Tserpes K, Tzatzadakis V, Katsiropoulos C. Effect of hygrothermal ageing on the interlaminar shear strength of carbon fiber-reinforced rosin-based epoxy bio-composites. Compos Struct 2019;226:111211. https://doi.org/10.1016/j.compstruct.2019.111211.

[33] Tserpes KI, Moutsompegka E, Murariu O, Bonnaud L, Chanteli A. Experimental investigation of the effect of hygrothermal aging on the mechanical performance of carbon nanotube/PA6 nanocomposite. Plast Rubber Compos 2017;46:239–44. https://doi.org/10.1080/14658011.2017.1318499.

[34] Atiqah A, Ansari MNM, Kamal MSS, Jalar A, Afeefah NN, Ismail N. Effect of alumina trihydrate as additive on the mechanical properties of kenaf/polyester composite for plastic encapsulated electronic packaging application. J Mater Res Technol 2020;9:12899–906. https://doi.org/10.1016/j.jmrt.2020.08.116.

[35] Höhne C-C, Blaess P, Ilinzeer S, Griesbaum P. New approach for electric vehicle composite battery housings: electromagnetic shielding and flame retardancy of PUR/UP-based sheet moulding compound. Compos Appl Sci Manuf 2023;167:107404. https://doi.org/10.1016/j.compositesa.2022.107404.

[36] D20 Committee. Test method for water absorption of plastics n.d. https://doi.org/10.1520/d0570-98r10e01.

[37] D30 Committee. Test method for moisture absorption properties and equilibrium conditioning of polymer matrix composite materials n.d. https://doi.org/10.1520/d5229_d5229m-14.

[38] Kitamoto K, Minakuchi S, Yokozeki T. High-fidelity simulation model for moisture-induced deformation of CFRP structure considering anisotropic nonlinear moisture absorption-desorption characteristics. Compos Appl Sci Manuf 2023;165:107324. https://doi.org/10.1016/j.compositesa.2022.107324.

[39] Pierron F, Poirette Y, Vautrin A. A novel procedure for identification of 3D moisture diffusion parameters on thick composites: theory, validation and experimental results. J Compos Mater 2002;36:2219–43. https://doi.org/10.1177/0021998302036019003.

[40] Li C, Dong Y, Yuan X, Zhang Y, Gao X, Zhu B, et al. Waterborne polyurethane sizing agent with excellent water resistance and thermal stability for improving the interfacial performance of carbon fibers/epoxy resin composites. Colloids Surf A Physicochem Eng Asp 2024;681:132817. https://doi.org/10.1016/j.colsurfa.2023.132817.

[41] Pavlidou S, Papaspyrides CD. The effect of hygrothermal history on water sorption and interlaminar shear strength of glass/polyester composites with different interfacial strength. Compos Appl Sci Manuf 2003;34:1117–24. https://doi.org/10.1016/S1359-835X(03)00214-8.

[42] Hassanpour B, Karbhari VM. Characteristics and models of moisture uptake in fiber-reinforced composites: a topical review. Polymers 2024;16:2265. https://doi.org/10.3390/polym16162265.

[43] Addepalli S, Zhao Y, Erkoyuncu JA, Roy R. Quantifying uncertainty in pulsed thermographic inspection by analysing the thermal diffusivity measurements of metals and composites. Sensors 2021;21:5480. https://doi.org/10.3390/s21165480.

[44] D20 Committee. Test methods for flexural properties of unreinforced and reinforced plastics and electrical insulating materials n.d. https://doi.org/10.1520/D0790-15.

[45] Li H, Zhang K, Fan X, Cheng H, Xu G, Suo H. Effect of seawater ageing with different temperatures and concentrations on static/dynamic mechanical properties of carbon fiber reinforced polymer composites. Compos B Eng 2019;173:106910. https://doi.org/10.1016/j.compositesb.2019.106910.

[46] Barjasteh E, Nutt SR. Moisture absorption of unidirectional hybrid composites. Compos Appl Sci Manuf 2012;43:158–64. https://doi.org/10.1016/j.compositesa.2011.10.003.

[47] Springer GS. Effects of temperature and moisture on sheet molding compounds. J Reinforc Plast Compos 1983;2:70–89. https://doi.org/10.1177/073168448300200201.

[48] Hu R-H, Sun M, Lim J-K. Moisture absorption, tensile strength and microstructure evolution of short jute fiber/polylactide composite in hygrothermal environment. Mater Des 2010;31:3167–73. https://doi.org/10.1016/j.matdes.2010.02.030.

[49] Pan Y, Zhong Z. Modeling of the mechanical degradation induced by moisture absorption in short natural fiber reinforced composites. Compos Sci Technol 2014;103:22–7. https://doi.org/10.1016/j.compscitech.2014.08.010.

[50] Wang J, Li Y, Li Q, Long Y, Yu T, Li Z. Evolution of stiffness in flax yarn within flax fiber reinforced composites during moisture absorption. Compos B Eng 2024;268:111096. https://doi.org/10.1016/j.compositesb.2023.111096.

[51] Ferreira Rocha PR, Fonseca Gonçalves G, Dos Reis G, Guedes RM. Mechanisms of component degradation and multi-scale strategies for predicting composite durability: present and future perspectives. J Compos Sci 2024;8:204. https://doi.org/10.3390/jcs8060204.

[52] Sang L, Wang C, Wang Y, Hou W. Effects of hydrothermal aging on moisture absorption and property prediction of short carbon fiber reinforced polyamide 6 composites. Compos B Eng 2018;153:306–14. https://doi.org/10.1016/j.compositesb.2018.08.138.

[53] Wang J, Gao J, Jiang J, Bi Y. Predicting degradation of composite-titanium adhesively bonded joints exposed to seawater environment. Eng Struct 2023;297:116993. https://doi.org/10.1016/j.engstruct.2023.116993.

[54] Fragiadaki A, Tserpes K. Impact response of a thermoplastic battery housing for transport applications. https://doi.org/10.20944/preprints202509.0996.v1; 2025.